Annu. Rev. Fluid Mech. 2005. 37:425–55
doi: 10.1146/annurev.fluid.36.050802.122052


# PRINCIPLES OF MICROFLUIDIC ACTUATION BY MODULATION OF SURFACE STRESSES

Anton A. Darhuber and Sandra M. Troian
*School of Engineering and Applied Science, Princeton University, Princeton, New Jersey 08544; email: darhuber@princeton.edu; url: www.princeton.edu/~stroian*



**Key Words** microfluidics, Marangoni stress, thermocapillary flow, textured surfaces, droplet actuation, micro-patterned flow

■ **Abstract** Development and optimization of multifunctional devices for fluidic manipulation of films, drops, and bubbles require detailed understanding of interfacial phenomena and microhydrodynamic flows. Systems are distinguished by a large surface to volume ratio and flow at small Reynolds, capillary, and Bond numbers are strongly influenced by boundary effects and therefore amenable to control by a variety of surface treatments and surface forces. We review the principles underlying common techniques for actuation of droplets and films on homogeneous, chemically patterned, and topologically textured surfaces by modulation of normal or shear stresses.

## 1. INTRODUCTION

Commercial interest in microfluidic devices for simultaneously propelling different liquids through individually addressable channels has grown considerably over the past decade (Thorsen et al. 2003). Such parallel operation accelerates automated synthesis and analysis of small liquid samples, significantly minimizing reagent volume and cost. Device manufacture has benefited from advances in silicon processing and MEMs technology to widespread use of inexpensive elastomeric polymers for surface patterning and encapsulation. Microfluidic devices are being used for such diverse applications as DNA microarrays, drug screening, optical display technologies, tunable fiber optic waveguides, thermal management of semiconductor devices and lasers, clinical and forensic analysis, and environmental monitoring.

Most fluidic devices generate internal flow through microchannels in glass or silicon using electro-osmosis (Stone et al. 2004), electrohydrodynamics (Bart et al. 1990), magnetohydrodynamics (Jang et al. 2000), centrifugation (Duffy et al. 1999), or pressure gradients (Pfahler et al. 1990). Driving mechanisms based on surface stresses, however, are particularly effective for free surface flows, given the large surface to volume ratio intrinsic to microscale systems. Controlled modulation of fluid-fluid or fluid-solid boundaries has been demonstrated using

electrowetting (Lee et al. 2000, Pollack et al. 2000), dielectrophoresis (Jones et al. 2001, 2004), thermocapillary (Darhuber et al. 2003b), and Marangoni stresses (Gallardo et al. 1999). Two distinct advantages of systems based on external flow are direct accessibility to liquid samples and a reduced contact area generating less friction at solid boundaries. The main disadvantage is evaporative loss, which can be minimized by encapsulation or by lowering the operating temperature. Irrespective of the driving mechanism, current emphasis is on development of inexpensive, robust, and portable units.

Development and optimization of fluidic devices based on free surface flow requires a fundamental understanding of interfacial phenomena and the influence of surface energy modulation. Most underlying interfacial phenomena were qualitatively understood by the end of the nineteenth century; however, to this day there remain many systems for which quantitative descriptions are still lacking. Interest in this subject today is focused on discrete or continuous microscopic control of small-scale systems. Experimental capabilities have been greatly extended through development of new techniques for chemical and topological patterning of substrates involving photolithography, selective material deposition and etching, or surface micromachining. Integrated microscale sensors and detectors have also enhanced the usefulness of these devices.

Predictions for the shape and speed of droplets and films require accurate models for the forces affecting the advance of the triple-phase contact line. This necessitates consideration of the difference between dynamic and static contact angles (Cox 1986, Dussan 1979, Shikhmurzaev 1997), contact angle hysteresis (Chen et al. 1991; Johnson & Dettre 1964, 1965), line tension (Rowlinson 1983), and the stress singularity caused by the no-slip condition (Cox 1986, Dussan 1976, Huh & Scriven 1971). Line tension is only significant for system sizes below about $10^{-2}$ $\mu$m (Adamson 1990) and is usually negligible in microscale flows. Hysteretic effects, however, greatly influence droplet mobilization because a critical force is required to overcome contact line pinning due to chemical, topological, or adsorptive defects. For contact line motion, the dynamic advancing contact angle, $\theta$, must exceed a minimum value, $\theta_A$, greater than its static value, $\theta_s$, i.e., $\theta > \theta_A \geq \theta_s$. Likewise, the dynamic receding contact angle must satisfy $\theta < \theta_R \leq \theta_s$ (Chen et al. 1991; Johnson & Dettre 1964, 1965). For a two-dimensional (2D) droplet with speed $U$, the hysteresis is characterized by $\theta_A(U) - \theta_R(U)$. The nonintegrable stress singularity at a moving contact line can be relieved by slip conditions (Greenspan 1978, Navier 1823), where the slip velocity is proportional to the local shear rate, by a precursor layer formed by evaporation/condensation processes at the contact line, or by adsorption of a molecular film (de Gennes 1985). Molecular dynamics simulations were recently used to explore the origin and dynamic response of the slip length (Barrat & Bocquet 1999, Priezjev & Troian 2004, Thompson & Troian 1997); these results have yet to be incorporated into continuum models.

This article provides an overview of physical mechanisms based on modulation of normal and shear stresses for fluidic actuation on homogeneous, chemically

patterned, or topologically textured surfaces. The majority of flows are investigated within the lubrication approximation (Leal 1992), for which the geometric aspect ratio, $\epsilon^2 = (h/L)^2 \ll 1$, and the dynamic ratio, $\epsilon \cdot \mathsf{Re} \ll 1$, where $\mathsf{Re}$ is the Reynolds number. Not included here is a description of electrokinetic phenomena, nor particle or droplet migration by electromechanical body forces such as dielectrophoresis (Jones et al. 2001). Additional issues relating to intermolecular forces, line tension, multiphase flow, evaporation and segregation, microscale mixing phenomena (Ottino & Wiggins 2004), or device fabrication are also not considered. In sections 2 and 3, we examine the influence of capillary forces on the static and dynamic behavior of films and droplets in response to chemically or topologically modified surfaces. Sections 4 and 5 are devoted to liquid actuation by variation of the fluid-fluid or fluid-solid interfacial tension.

## 2. STATIC CAPILLARY PHENOMENA

The equilibrium shape, $h(x, y)$, of an isothermal liquid droplet of constant volume, $V$, resting on a flat solid (in an ambient vapor phase of negligible density) is determined by minimizing the total free energy, $E - pV$, which includes all contributions from body, surface, or line forces. Here, $p$ is the total pressure within the liquid phase. The surface contribution is given by $\gamma_{lv}A_{lv} + \gamma_{ls}A_{ls} + \gamma_{sv}A_{sv}$, where $\gamma_{ij}$ and $A_{ij}$ denote the interfacial tensions and contact areas between the liquid-vapor ($lv$), liquid-solid ($ls$), and solid-vapor ($sv$) boundaries. The Young-Laplace equation specifies the pressure drop across a curved liquid-vapor interface according to $-\gamma_{lv}\nabla_s \cdot \mathbf{n} = -\gamma_{lv}(1/R_1 + 1/R_2)$, where $R_{1,2}$ represent the local principal radii of curvature characterizing the $lv$ interface. In a gravitational field, mechanical equilibrium requires that $\gamma_{lv}(1/R_1 + 1/R_2) + \rho g z = const$, where $\rho$ is the liquid density, $g$ is the gravitational constant, and $z$ is the vertical distance from the solid surface $z = 0$. For small slopes, both $|\partial h/\partial x|^2 \ll 1$ and $|\partial h/\partial y|^2 \ll 1$ and the surface gradient, $\nabla_s = \nabla - \mathbf{n}(\mathbf{n}\cdot\nabla)$, simply reduces to $(\partial/\partial x, \partial/\partial y)$, where $\mathbf{n}$ is the outward oriented unit normal at the $lv$ interface. In this limit, the capillary pressure simplifies to $p = -\gamma_{lv}(\partial^2 h/\partial x^2 + \partial^2 h/\partial y^2)$. The angle of contact, $\theta_s$, at the three-phase boundary is specified by the Young-Dupré condition, $\gamma_{lv}\cos\theta_s = \gamma_{sv} - \gamma_{ls}$. In this article, the term nonwetting refers to angles $\theta_s > \pi/2$, partially-wetting to angles $\theta_s < \pi/2$, and completely wetting to $\theta_s = 0$. In general, the computation of liquid shapes on textured surfaces can lead to complicated analytic expressions; however, the availability of software packages like Surface Evolver (Brakke 1992) greatly simplifies the numerical computation of minimum energy surfaces subject to complex surface or volumetric constraints.

### 2.1. Droplet Shapes on Chemically Patterned Surfaces

A partially wetting droplet of characteristic dimension $L$ resting on a flat and chemically homogeneous substrate assumes the shape of a spherical cap provided $\mathsf{Bo} = \rho g L^2/\gamma_{lv} \ll 1$. For $\mathsf{Bo} \gtrsim 1$ [or equivalently $L \gtrsim \ell_c = \sqrt{\gamma_{lv}/\rho g}$, where $\ell_c$

is the capillary length (typically 1–3 mm)], hydrostatic forces flatten the droplet shape and the apex height is a nonmonotonic function of volume (Finn 1986). In the absence of evaporative or compositional effects, these configurations are stable. By contrast, liquid dispensed in the shape of a long and slender ribbon can undergo a Rayleigh instability if the contact lines are free to move. Davis (1980), using a hydrodynamic analysis, and Sekimoto et al. (1987), using energy-minimizing arguments, examined the linear stability of infinitely long liquid rivulets subject to various boundary conditions at the contact lines. For immobile lines, a liquid ribbon is unconditionally stable provided $\theta_s < 90^\circ$ (Davis 1980). For $90^\circ < \theta_s < 180^\circ$, the ribbon is linearly stable to longitudinal disturbances of wavenumber $k$ provided $(kR)^2 > 3/4$, where $R$ is the unperturbed radius of curvature. Roy & Schwartz (1999) used energy minimization to examine the stability of liquid ribbons within hollow wedges or circular and ellipsoidal cylinders. For a given substrate geometry and contact angle, stability is guaranteed provided the unperturbed meniscus pressure is an increasing function of the liquid cross-sectional area.

Well developed surface treatments exist for patterning surfaces like gold, silicon, or glass into regions of mixed wettability. The surface energy can be modified, for example, by selective adsorption of self-assembling monolayers consisting of alkylthiol or chlorosilane molecules (Maoz & Sagiv 1984). The critical surface tension of perfluorinated coatings is among the lowest measured (Shafrin & Zisman 1960), producing water contact angles up to 119° on flat and smooth surfaces. The large contrast in contact angle between uncoated ($\theta_s = \theta_{\text{int}}$) and coated ($\theta_s = \theta_{\text{ext}}$) regions helps confine liquid films or droplets to the more wettable regions of a substrate. The Young-Dupré equation does not hold if a contact line coincides with the boundary (B) differentiating the regions characterized by $\theta_{\text{int}}$ from $\theta_{\text{ext}}$. In this case, $\theta_B$ can assume any value between $\theta_{\text{int}}$ and $\theta_{\text{ext}}$, depending on the liquid volume and boundary geometry. This effect, which is known as canthotaxis (Langbein 2002), can also occur along sharp edges between planes of equal surface energy.

Gau et al. (1999) and Darhuber et al. (2000a) investigated the static conformation of liquid ribbons and droplets on chemically heterogeneous surfaces. Figure 1*a*,*b* illustrates the equilibrium shapes on a partially wetting rectangular stripe for the case $\theta_{\text{ext}} = 180^\circ$ and $\theta_{\text{int}} = 60^\circ$ or $30^\circ$. With increasing volume, the droplet elongates along the stripe for $\theta_{\text{int}} = 30^\circ$, whereas it develops a bulge for $\theta_{\text{int}} = 60^\circ$. Brinkmann & Lipowsky (2002) found that elongated ribbons of essentially constant cross-section only form if $\theta_{\text{int}} < \arccos(\pi/4) \approx 38^\circ$ and $\theta_{\text{ext}} \geq 90^\circ$ for sufficiently large volumes. Gau et al. (1999) observed the formation of a single bulge for completely wetting liquids and sufficiently large volumes, i.e., $\theta_B > 90^\circ$ (Figure 1*c*). Moreover, a corner formed by the intersection of two wettable stripes can induce a bulge (Figure 1*d*,*e*), which can be eliminated by smoothing the corner (Figure 1*f*,*g*). In general, liquids on chemically structured surfaces can undergo abrupt shape transitions with increasing volume. Brinkmann & Lipowsky (2002) computed bifurcation diagrams and stability limits for a number of interesting surface patterns.

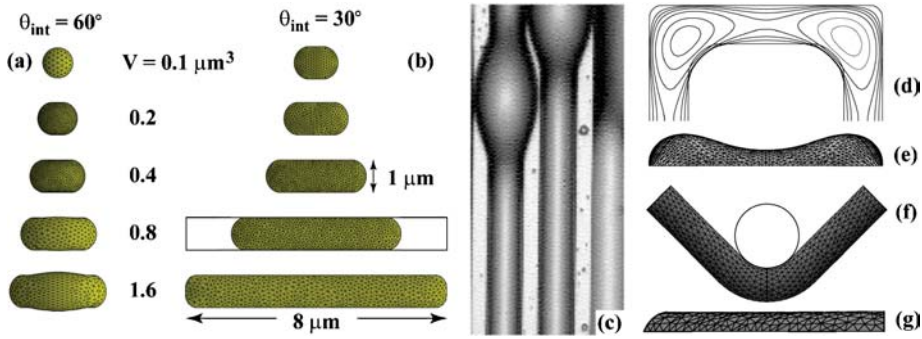


**Figure 1** (*a*,*b*) Simulation results of sessile droplets of volume $V = 0.1$–$1.6\,\mu\text{m}^3$ on a rectangular microstripe of dimensions $1\,\mu\text{m} \times 8\,\mu\text{m}$. Exterior contact angle $\theta_{\text{ext}} = 180^\circ$; interior contact angle (*a*) $\theta_{\text{int}} = 60^\circ$ and (*b*) $30^\circ$ (Darhuber et al. 2000a). (*c*) Ribbons of water condensed from the vapor phase on hydrophilic microstripes about $50\,\mu\text{m}$ in width. Above a critical volume such that $\theta_B > 90^\circ$, a bifurcation from uniform cross-section to a single bulge occurs, unlike a Rayleigh instability. [Reprinted with permission from Gau et al. (1999). Copyright AAAS.] (*d*,*e*) Top (contour) and side views of a liquid ribbon on a half loop pattern measuring $10\,\mu\text{m}$ in length with $\theta_{\text{int}} = 45^\circ$ and $\theta_{\text{ext}} = 135^\circ$. Liquid accumulates near the corners (Darhuber et al. 2000a). (*f*,*g*) Top and side views of a $10\,\mu\text{m}$ wide liquid ribbon on a rounded corner pattern with $\theta_{\text{int}} = 0^\circ$ and $\theta_{\text{ext}} = 180^\circ$. When the inner radius of curvature (indicated by the circle) is made to equal the microstripe width, bulges are eliminated for moderate fill volumes, and the liquid height profile becomes uniform (Darhuber et al. 2000a).

For a prescribed set of interfacial energies, the pattern feature size, such as the width $w$ of the microstripes shown in Figure 1, can be used to control the liquid shape for $w \ll \ell_c$. As a consequence of the equilibrium condition of constant mean curvature, the characteristic liquid thickness scales as $h \sim w^2$ because $\partial^2 h/\partial x^2 + \partial^2 h/\partial y^2 \sim h/w^2 = const$. The length scale $w$ also determines the lateral scale governing the drop-off in film height near boundaries or nonwetting defects (Darhuber et al. 2001a). Incorporation of line tension or disjoining pressure effects will introduce additional length scales, which can modify the equilibrium conformations and stability limits on chemically decorated surfaces.

## 2.2. Droplet Shapes on Topologically Textured Surfaces

Textured surfaces can be categorized into those that have sharp corners and edges and those whose slopes and curvatures vary smoothly with position. Concus & Finn (1974) first studied the equilibrium shape of a finite volume of liquid inside a wedge with opening angle $\beta$, where the contact angles on the two intersecting half planes are $\theta_1$ and $\theta_2$. For the symmetric case $\theta_1 = \theta_2$ and small opening angle $\beta < \pi - 2\theta_1$, there is no stable equilibrium shape because the liquid is continuously wicked along the wedge. Nonwetting liquids for which $2\theta_1 > \pi + \beta$ instead form a

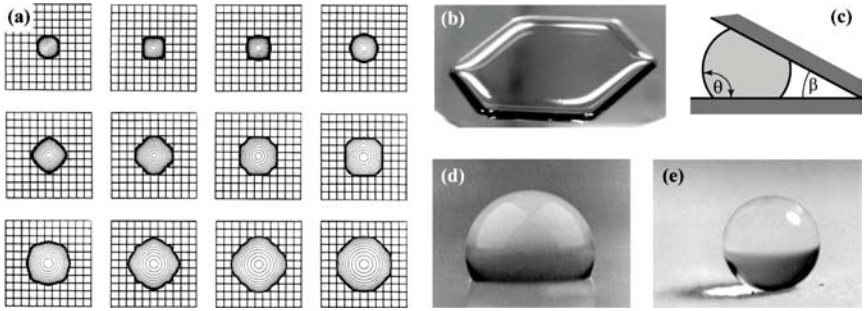


**Figure 2** (*a*) Contour plots of the equilibrium shape of sessile droplets on a corrugated surface with increasing volume (Huh & Mason 1977). (*b*) Glycerol/water droplet (diameter 6 cm) on an hexagonal array of hydrophobic defects of thickness 0.5 $\mu$m, diameter 400 $\mu$m and pitch 707 $\mu$m (Cubaud & Fermigier 2001). (*c*) Liquid bridge formed by a droplet between two nonwetting intersecting surfaces. (*d*,*e*) Water droplet on a (*d*) smooth ($\theta = 109^\circ$) and (*e*) rough ($\theta = 174^\circ$) alkylketene dimer substrate with a fractal dimension of 2.29. [Reprinted with permission from Onda et al. (1996). Copyright Am. Chem. Soc.]



spherical bridge as shown in Figure 2*c*. Gibbs (1906) realized that sharp edges and steps can also be used to confine liquids and pin contact lines. Mori et al. (1982) demonstrated that liquid spreading can be inhibited by step heights as small as 60 nm on cleaved mica.

Huh & Mason (1977) examined droplet shapes for partially wetting liquids on a corrugated surface, $s(x, y) = \varepsilon l \sin(\pi x/l) \sin(\pi y/l)$, by a perturbation analysis of the Young-Laplace equation. As shown in Figure 2*a* for $\theta = 40^\circ$, even small-amplitude corrugations ($\varepsilon = 0.05$) can induce pronounced distortion from axisymmetry. The droplet equilibrium center positions coincide with local minima of the doubly grooved surface. Similar polygonal shapes are adopted by liquid droplets on surfaces patterned by an array of nonwetting defects (Figure 2*b*) or arrays of cylindrical pillars (Krupenkin et al. 2004). In these examples, the surface protrusions are more than two orders of magnitude smaller in diameter than the droplets.

Surface textures with large geometric aspect ratios can generate super-wettable or super-nonwettable substrates. As shown in Figure 2*d*,*e*, the contact angle $\theta$ of a water droplet on a hydrophobic waxy surface can be increased from 109° to 174° by roughening the surface. As a consequence of air entrapment in crevices, only a fraction of the supporting solid is in direct contact with the liquid phase. For a liquid film on a mesh or screen where $f_1$ is the area fraction of liquid in contact with the mesh and $f_2$ the area fraction in contact with air, Cassie & Baxter (1944) showed that $\cos\theta = f_1 \cos\theta_1 - f_2$. Ollivier (1907) first reported this effect for water droplets on hydrophobic powders; lotus leaves and duck's feathers (Moilliet 1963) repel rain droplets for the same reason. Nowadays, synthetic, highly

water-repellent surfaces, called superhydrophobic or ultrahydrophobic (Busscher et al. 1992, Kunugi et al. 1993), can be fabricated from different materials including silicon nanoposts (Krupenkin et al. 2004) or aligned carbon nanotubes coated with a hydrophobic layer of poly(tetrafluoroethylene) (Lau et al. 2003).

## 3. DYNAMICAL CAPILLARY PHENOMENA

Spatial variations in the capillary pressure can be used to pump small liquid volumes over sizeable distances. Common manifestations include liquid imbibition into closed or open channels and droplet propulsion between tilted substrates. In this section, both "passive" and "active" capillary techniques, which are well suited to microfluidic applications, are reviewed.



### 3.1. Capillary Wicking in Enclosed Channels

The general equation for the position of a gas-liquid interface, $L(t)$, advancing with time $t$ inside a vertical capillary of cross-sectional area $A_c$ and perimeter $P_c$ is given by $-{L_e}^2 \ln(1 - L/L_e) - L_e L = f\gamma_{lv} P_c \cos\theta\, t/\mu$, where $\mu$ is the liquid viscosity, $f$ is a geometric coefficient depending on the conduit geometry, and $L_e = \gamma_{lv} P_c \cos\theta/(\rho g A_c)$ is the final equilibrium height determined by the balance of surface tension and gravity (Langbein 2002, Lucas 1918). For $L(t) \ll L_e$, Washburn (1921) confirmed by analysis and experiment that $L(t) = (2f\gamma_{lv} P_c \cos\theta\, t/\mu)^{1/2}$. The Washburn equation also describes the advance of the liquid for all times into horizontal capillaries or capillaries of arbitrary orientation in microgravity conditions. Corrections involving entry and inertial effects at early times or dynamic contact angles are described by Middleman (1995). The negative capillary pressure at the moving front caused by the meniscus curvature is responsible for the advance of the liquid. The $t^{1/2}$ scaling is a direct consequence of the fact that the pressure gradient driving the flow is independent of the length of the liquid column $L(t)$. Krotov & Rusanov (1999) compared wicking rates in capillaries of circular, triangular, and circular-triangular shapes of equal cross-sectional area and found that the rate of penetration is highest for the latter geometry.

### 3.2. Capillary Spreading Along Surface Grooves

Microscopic roughness can significantly enhance the wicking capability of surfaces. Raphaël (1989) studied the capillary rise of liquid along a semicircular and completely wettable groove of radius $R$. In the absence of van der Waals forces and liquid surface curvature along the spreading direction within the lubrication limit, the governing equation for the film thickness, $h(x, t)$, reduces to a nonlinear diffusion equation in the similarity variable $\eta = x/\sqrt{(\gamma_{lv} R/\mu)t}$ provided gravitational drainage is negligible. Summ et al. (1980) and Mann et al. (1995) investigated the spreading of liquids along a V groove with opening angle $\beta$ and found that the

liquid front advances with the Washburn-like scaling, $L \sim [\gamma_{lv} h_0 K(\beta, \theta)\, t/\mu]^{1/2}$, where $h_0$ is the liquid height at the entry to the groove and $K(\beta, \theta)$ is a geometric factor. Excellent agreement was obtained between experiment and theory. A more detailed and rigorous analysis of flow in horizontal V grooves using similarity methods was provided by Romero & Yost (1996) and Weislogel & Lichter (1998).

Capillary wicking is integral to the technology of heat pipes (Faghri et al. 1993), which can sustain axial heat fluxes up to 20 kW/cm$^2$ (Dunn & Reay 1978), and hot-spot mitigation for cooling of high-power semiconductor devices and lasers. The efficiency of liquid wicking at even smaller length scales has led to significant interest in channels formed by carbon nanotubes or polymeric nanofibers coated with biosensitive molecules (Neimark et al. 2003).



## 3.3. Capillary Spreading on Wettable Microstripes

Wicking phenomena in open conduits is not limited to concave liquid shapes. Liquid films spontaneously advance along narrow wettable stripes of width $w$, according to the Washburn scaling $L \sim t^{1/2}$. Darhuber et al. (2001a) examined a hydrodynamic model for the isothermal, capillary spreading of a liquid ribbon with small aspect ratio emanating from a square reservoir pad in the limit $h \ll w \ll L(t)$, as sketched in Figure 3*a*. The equation governing the evolution of the film height, $h(x, y, t)$, is given by $\partial h/\partial t - \nabla \cdot \left[h^3 \nabla p/(3\mu)\right] = 0$, where $p = -\gamma_{lv}(\partial^2 h/\partial x^2 + \partial^2 h/\partial y^2)$ is the capillary pressure and $h^3 \nabla p/(3\mu)$ is the volumetric flow rate per unit width. For $w \ll L$ and away from the advancing front, $\partial p/\partial y \approx \partial^3 h/\partial y^3 \approx 0$ because the transverse flux vanishes at the stripe edge. To excellent approximation, the transverse profile is a parabola, $h(x, y, t) = h_c(x, t)(1 - 4y^2/w^2)$, where $h_c = h(x, y = 0, t)$ is the maximum thickness along the stripe centerline. The dominant contribution to the pressure gradient is therefore $\partial p/\partial x = -\gamma\, \partial^3 h/\partial x \partial y^2 = 8\gamma(\partial h_c/\partial x)/w^2$. The evolution equation reduces to a second-order nonlinear diffusion equation for $h_c$. A similarity solution can be obtained in the transformed coordinates $\Phi = h_c/h_0$ and $\eta = x/\sqrt{Dt}$, where $D = (64/35)\gamma_{lv} h_0^3/(\mu w^2)$ and $h_0$ is the film thickness at the stripe inlet (Figure 3*a*). Consequently, the liquid advances according to $L(t) \sim \sqrt{Dt}$ (or equivalently $dL/dt \propto L^{-1}$). The length scale that appears in the coefficient $D$ is given by the ratio $h_0^3/w^2$, in contrast to the capillary radius $R$ in the Washburn problem. The experimental results shown in Figure 3*c* confirm that the propagation speed decreases as $L^{-1}$ when the liquid front has advanced sufficiently far downstream that the streamwise curvature is negligible. For sufficiently large reservoir pads, such that the inlet height remains constant, the film height scales as $h_0 \sim w^2$ (Darhuber et al. 2001a) and the speed of advance as $dL/dt \sim w^4/L(t)$. This relation between the inlet height and the feature size establishes a much stronger (quartic) dependence of the propagation speed on the length scale $w$, as confirmed by experiment (Figure 3*d*). By contrast, Washburn's equation for enclosed channels predicts $dL/dt \sim R/L(t)$.

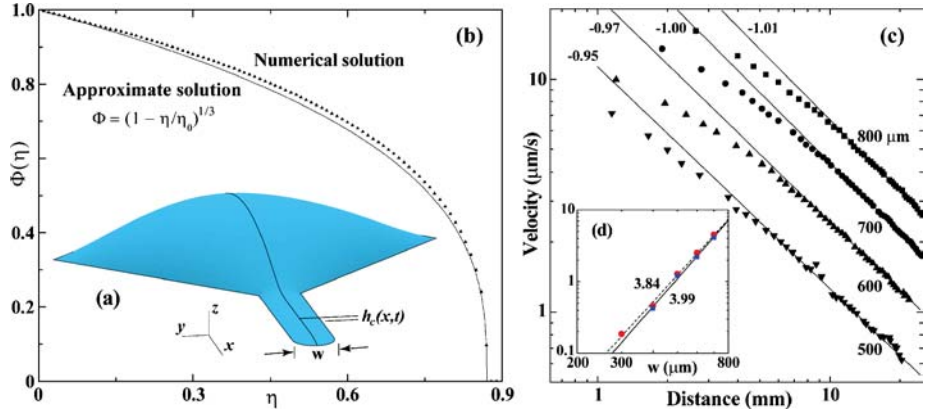


**Figure 3** (*a*) Diagram of hydrophilic reservoir pad and confining stripe geometry for studies of isothermal capillary spreading. Inlet position at $x = 0$ (Darhuber et al. 2003a). (*b*) Self-similar solutions for the normalized film thickness profile, $\Phi(\eta) = h/h_0$, of a spreading rivulet. Dotted line, numerical solution; solid line, approximate analytic solution (Darhuber et al. 2001a). (*c*) Measurements of the propagation speed of silicone oil rivulets ($\mu = 20\,m$Pa s) with distance. Solid lines; power law fits with exponents indicated for $500 \leq w \leq 800\,\mu$m (Darhuber et al. 2001a). (*d*) Measurements of the propagation speed versus stripe width, $w$, at fixed position $x = 10$ mm from the inlet. Solid lines: power law fits for two experimental runs (Darhuber et al. 2001a).

The contribution to the pressure gradient due to the transverse interfacial curvature strongly depresses the film thickness in many spreading and coating flows at low Ca. For example, liquid confinement to a narrow stripe sharply decreases the controlling length scale ($\sqrt{\gamma_{lv}/\rho g} \to w$) and dynamic scaling ($\mathrm{Ca}^{2/3} \to \mathrm{Ca}^{1/3}$) for the entrained thickness in dip-coating processes (see Appendix).

## 3.4. Propulsion by Capillary Pressure Gradients

Instead of the spontaneous flow described above, active manipulation can be achieved by establishing either a difference in the surface tension or the radius of curvature at the ends of a liquid plug. In the simplest example, droplets bounded by nonparallel surfaces can be moved on demand with a prescribed speed and direction. Hauksbee (1712) described the motion of a wetting droplet sandwiched in-between flat and nonparallel plates (Figure 4*a*). He observed that the liquid moved toward the converging end with increasing speed. In the same fashion, a plug in an open conical tube migrates toward the cone tip (Bouasse 1924) for wetting liquids. Weislogel (1997) investigated a similar effect in capillary tubes whose interior surfaces were partially coated to induce differences in contact angle. A bislug consisting of two immiscible liquids of different surface tension within a capillary behaves analogously. Marangoni (1871) reported the


**Figure 4** (*a*) A liquid plug with $\theta < 90^\circ$ ($\theta > 90^\circ$) moves toward (away from) the narrow gap region. (*b*) A self-propelled bislug ($\gamma_{12} = 18.0$ mN/m) of ethylene glycol ($\gamma_1 = 47.7$ mN/m) and silicone oil ($\gamma_2 = 20.3$ mN/m) in a 1 mm diameter glass capillary. [Reprinted from Bico & Quéré (2002) with permission from Cambridge Univ. Press.]



spontaneous motion of a water-carbondisulfide bislug in a glass capillary. Bico & Quere (2002) recently conducted an experimental study of liquid bislugs in capillary tubes including consideration of film entrainment (Figure 4*b*). Bislug motion requires that one of the liquids be completely wetting. The difference in capillary pressure driving the motion for completely wetting menisci is $\Delta p = \frac{2}{R}(\gamma_1 - \gamma_{12} - \gamma_2)$, where $\gamma_{1,2}$ is the surface tension of the liquids in the slug and $\gamma_{12}$ is the mutual interfacial tension.

An electronically addressable method of propelling small liquid plugs for microfluidic applications was developed by Sammarco & Burns (1999). The capillary pressure at the advancing (A) and receding (R) ends of the plug is tuned by activating heating resistors (whose width is smaller than the droplet length) embedded within the supporting substrate. The speed of a plug of length $L$ subject to a temperature difference between the advancing and receding droplet edges, $\Delta T = T_R - T_A$, moving through a horizontal capillary of diameter $d$ in the absence of an external pressure gradient, is given by $U = f\, b\, d \cos\theta_R\, (\Delta T - \Delta T_{\min})/(\mu\, L)$. Here, the constant $b$ is defined by $\gamma_{lv} = a - bT$, $f$ is a geometric factor, and $\Delta T_{\min}$ is the minimum thermal difference required for droplet mobilization due to contact angle hysteresis, i.e., $\theta_A - \theta_R \neq 0$. Makihara et al. (1999) devised a photonic switch based on this method of thermocapillary propulsion. Light propagating through a waveguide is deflected by the presence of a gas bubble or oil plug in a liquid-filled channel, which is actuated by thermocapillary pumping.

## 4. PROPULSION BY SUBSTRATE ENERGY GRADIENTS

The direction and speed of droplets along a solid substrate can be controlled by modulating the interfacial energy between the solid and liquid phases by means of chemical surface composition gradients or electrowetting. The propulsion mechanism relies on the difference in contact angle between the advancing and trailing ends. The region near the moving contact lines provides the source of energy for propulsion, in contrast to droplet migration on homogeneous surfaces, where this region is mostly dissipative.

### 4.1. Motion on Chemically Nonuniform Surfaces

Greenspan (1978) developed a lubrication model for the motion of a small viscous droplet on either chemically homogeneous or heterogeneous surfaces. He was

interested in capillary spreading and retraction, the distortion of biological cells owing to surface contamination, and the creeping motion of a cell or droplet on chemically graduated surfaces. For small equilibrium contact angles, $\theta_s$, he assumed that the contact line ($cl$) advances with velocity $\mathbf{v}_{cl} = \kappa(\theta - \theta_s)\,\hat{\mathbf{n}}$ and invoked a slip condition along the liquid-solid interface of the form $\mathbf{v}(z=0) = \alpha/(3h)(\partial\mathbf{v}/\partial z)$, where the coordinate axis $\hat{z}$ is perpendicular to the substrate. Here, $\theta$ is the dynamic contact angle, $\hat{\mathbf{n}}$ the outward unit normal vector to the contact line in the plane of the substrate, and $\alpha$ a constant of order $10^{-10}\,\mathrm{cm}^2$. Neglecting contact angle hysteresis and disjoining pressure effects, he showed that

$$\frac{\partial h}{\partial t} + \frac{\gamma}{3\mu}\nabla\cdot\left[h(h^2+\alpha)\nabla(\nabla^2 h)\right] = 0. \tag{1}$$

Greenspan solved this equation for the case of a droplet slowly spreading on a chemically graduated surface characterized by $\theta(\tilde{x}) = (1-\tilde{\lambda}\tilde{x})\,\theta_0$, where $\tilde{\lambda} \ll 1$. Nondimensionalization of Equation 1 by $(\tilde{x}, \tilde{y}) = (x/R_0,\ y/R_0)$, $\tilde{h} = h/(\theta_0 R_0)$, $\tilde{t} = \kappa\theta_0 t/R_0$, and $\tilde{\mathbf{v}} = \mathbf{v}/(\kappa\theta_0)$, where $R_0$ is the initial droplet radius and $\theta_0$ is the initial static contact angle, causes the time-dependent term to scale linearly with the small parameter $\epsilon \equiv 3\mu\kappa/(\theta_0^2\gamma_{lv})$. From a perturbation expansion of the height profile, he concluded that to zero order the droplet maintains a spherical cap shape and moves with an average speed $U = \kappa\theta_0 R_0\lambda = -\kappa R_0(d\theta/dx)$. The droplet therefore migrates toward regions of smaller contact angle or equivalently regions of greater adhesion. The liquid viscosity does not explicitly appear in this expression because $h_0$ is a surface of constant curvature, i.e., $\nabla p = 0$. The droplet only moves by virtue of the imposed contact line condition for $\mathbf{v}_{cl}$.

Brochard (1989) used a force balance at the liquid-solid interface to derive an expression for the motion of a 2D droplet along a substrate with a variation in the spreading coefficient, $dS/dx = d\gamma_{sv}/dx - d\gamma_{ls}/dx \neq 0$. Within the lubrication limit, the droplet speed was determined to be

$$U = (S_B - S_A)\left/\left[3\mu\int_A^B \frac{1}{h}\,dx\right]\right. = \frac{1}{3\mu\langle h^{-1}\rangle}\frac{dS}{dx}. \tag{2}$$

The second equality requires that $dS/dx = const$; $A$ and $B$ designate the position of the receding and advancing contact lines, respectively. To avoid the divergence in $\langle h^{-1}\rangle$ at the contact lines where $h=0$, Brochard introduced a cutoff length $x_{\min}$ of molecular dimension. From the Young-Dupré equation, $S$ can be expressed as $\gamma_{lv}(\cos\theta - 1)$, which yields $U = -\gamma_{lv}\sin\theta/(3\mu)(1/\langle h^{-1}\rangle)\,(d\theta/dx)$. Both models therefore predict that the droplet speed is proportional to $d\theta/dx$; however, because the opposing force due to contact angle hysteresis is neglected, these predictions only provide an upper bound on the speed.

Chaudhury & Whitesides (1992) and Daniel & Chaudhury (2002) prepared surfaces with graduated surface energy by grafting a monolayer of decyltrichlorosilane with decreasing surface density on glass and silicon substrates. Water droplets deposited on these surfaces spontaneously move uphill against the force of gravity

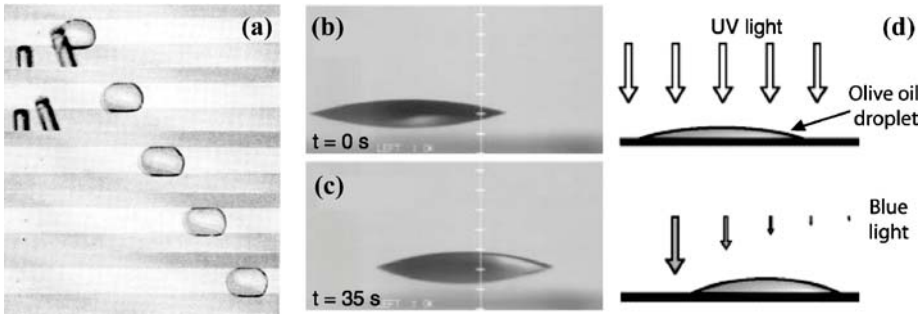


**Figure 5** (*a*) Image sequence ($\Delta t = 0.1$ s) of a reacting, self-propelled n-alkane droplet containing perfluorodecyltrichlorosilane on a 3 mm wide hydrophilic stripe. [Reprinted with permission from Dos Santos & Ondarçuhu (1995).] (*b–d*) Schematic diagram and photographs of droplet propulsion (olive oil) caused by asymmetric irradiation of an azobenzene photoisomerizable monolayer. UV (365 nm) light converts 90% of the monolayer to a *cis* conformation with a higher dipole moment (lower $\theta$); subsequent irradiation by blue light (436 nm) reverts the monolayer to the *trans* conformation (higher $\theta$). [Reprinted with permission from Ichimura et al. (2000). Copyright AAAS.]



toward regions of lower contact angle. The contact angle decreased by about 60° over a distance of 1 cm. Despite the fact that the contact angle hysteresis ranged from 10–20°, droplets of ethylene glycol ($\mu \approx 20$ mPa s) advanced with speeds up to 2 mm/s. Ichimura et al. (2000) coated a quartz substrate with a self-assembled monolayer containing photochromic azobenzene groups. Upon UV irradiation, the molecules transform from a planar *trans* configuration, which exposes the hydrophobic backbone, to a twisted *cis* configuration, in which the polar azo groups are exposed. The orientational change increases the value of $\gamma_{ls}$, which produces a corresponding change in the liquid contact angle (Ishihara et al. 1982). Ichimura et al. (2000) also demonstrated that asymmetric irradiation of a substrate can be used to propel a droplet (Figure 5*b–d*).

Gradients in the interfacial energy, $\gamma_{ls}$, can also be generated dynamically by a moving droplet containing a dissolved reagent that adsorbs to the substrate. Bain et al. (1994) and Dos Santos & Ondarçuhu (1995) examined self-propulsion of alkane droplets containing a perfluorinated carboxylic acid or perfluorodecyltrichlorosilane, which adsorbs onto the glass during motion. The trailing monolayer renders the surface hydrophobic. Droplet speeds in excess of a few centimeters per second were obtained in such "autophobic" (Hare & Zisman 1955) systems.

A small solid object can be propelled along a liquid surface in the same fashion by creating inhomogeneities in the spreading coefficient along its perimeter. The net force on the object due to surface tension variations is given by $\mathbf{F} = \oint_C \gamma_{lv} \mathbf{t}_n dl$, where $\mathbf{t}_n$ is the unit vector tangent to the liquid-vapor interface and normal to the three-phase contact line $C$. A well-known example of this effect is the dance of camphor scrapings on water, a phenomenon that puzzled observers for centuries

until van der Mensbrugghe properly explained the effect in 1869 (Rayleigh 1890). There is a renewed interest in camphor boats (Marcelin 1925) as a means of chemo-mechanical energy conversion (Nakata et al. 1997).

## 4.2. Electrocapillary Phenomena

Electrocapillarity refers to the modification of the interfacial tension at a fluid-fluid boundary by the presence of electrical charges. Lippmann (1875) constructed a capillary electrometer that contained a mercury-electrolyte (Hg-el) meniscus in a capillary tube subject to an externally applied voltage $V$. This apparatus was used to explore changes in the interfacial tension, $\gamma_{\mathrm{Hg,el}}$, as a function of $V$. With increasing voltage, he observed that the curves $\gamma_{\mathrm{Hg,el}}(V)$ were approximately parabolic in shape, first increasing toward a maximum and then decreasing. From thermodynamic considerations, Lippmann (1875) and Helmholtz (1882) derived the relation $(\partial\gamma_{\mathrm{Hg,el}}/\partial V)_\mu = -\sigma$, where $\sigma$ represents the surface charge density and the subscript $\mu$ denotes conditions of constant chemical potential. This relation essentially describes the reduction in surface tension due to Coulombic repulsion of the surface charges. Assuming the differential capacitance of the electrical double layer, $C = \partial\sigma/\partial V$, is a constant, it follows that $\gamma_{\mathrm{Hg,el}}(V) = \gamma^0_{\mathrm{Hg,el}} - C(V - V_{pzc})^2/2$. Here, $\gamma^0_{\mathrm{Hg,el}}$ designates the maximum interfacial tension obtained for an uncharged interface and $V_{pzc}$ is the applied voltage corresponding to the point of zero charge (pzc).

The spreading of electrolyte droplets on mercury is also affected by application of an external potential. Burdon & Oliphant (1927) reported that distilled water spread only very slowly on mercury, inorganic bases spread not at all, but very dilute acidic solutions spread very rapidly to a certain size and then stopped. Measurements indicated that the final contact area correlated with an approximate value of 1 elementary charge per nm$^2$. Droplets can be made to spread further or contract to a given size by applying an external voltage.

Möller (1908), Kabanov & Frumkin (1933), and Smolders (1961) conducted contact angle measurements of gas bubbles at mercury-electrolyte interfaces and found that the curves $\theta(V)$ resembled the electrocapillary curves for $\gamma_{\mathrm{Hg,el}}(V)$. They argued that a change in the interfacial energy proportional to $CV^2/2$ would be accompanied by a decrease in $\cos\theta$, according to the Young-Dupré equation. Subsequent studies using solid metal electrodes, silver iodide, and surface-modified quartz confirmed that the contact angle of bubbles depends on the surface charge density and assumes its maximum value at the pzc (Billet et al. 1976, Kabanov & Frumkin 1933, Laskowski & Kitchener 1969). The modification of contact angles by electrical charge effects is called electrowetting.

Fokkink & Ralston (1989) and Chatelier et al. (1995) present theoretical models for contact angles of electrolytes on charged and ionizable surfaces using the Guoy-Chapman theory of electrical double layers. They calculated the change in $\gamma_{ls}$ caused by a surface charge density for an infinite system, i.e., in the absence of a contact line. The Young-Dupré equation was then used to compute the modified contact angle assuming no change in $\gamma_{lv}$ and $\gamma_{sv}$. Digilov (2000) and Chou (2001)

were concerned that the presence of a contact line at a charged surface might induce effects not accounted for by this simple substitution. Digilov concluded that the applied potential causes polarization of the interface and the three-phase contact line, which reduces both the interfacial tension and the line tension. Chou modeled a 2D electrolyte droplet embedded in an immiscible electrolyte medium and residing on a solid substrate. He assumed constant surface charge densities on the interior ($\sigma_{1s}$) and exterior ($\sigma_{0s}$) solid surfaces. From minimization of the total free energy with respect to the position of the contact line and the droplet shape, he derived the modification in contact angle due to charge effects, namely $\gamma_{01}\cos\theta = \gamma_{0s} - \gamma_{1s} + (\sigma_{0s} - \sigma_{1s})\,\varphi(\theta)$, as well as the general equation describing the droplet shape. Here, $\gamma_{ij}$ denotes the interfacial tension between phases 0, 1, and s (solid) in the absence of electrostatic interactions, and $\varphi(\theta)$ is the electrical potential at the contact line, for which Chou provided approximate solutions in the limits $\kappa_0/\kappa_1 \to 1$ or $\kappa_0/\kappa_1 \to 0$. According to his derivation, any deviation from a simple wedge shape at the contact line occurs beyond a distance corresponding to the Debye screening lengths $\kappa_{0,1}^{-1}$.

4.2.1. ELECTROWETTING ON DIELECTRIC SUBSTRATES Solid electrode surfaces are often rough and chemically heterogeneous due to oxide layers and contaminant residues from the fabrication process, which can compromise reproducibility. If, however, an electrolyte solution is kept separated from the electrode surface by a thin, chemically inert, and electrically insulating (dielectric) layer, electrochemical reactions and specific adsorption are largely suppressed. This is advantageous for microfluidic applications as a large number of different liquids, electrolytes, and electrode materials can be used to generate qualitatively similar behavior.

In one of the first experiments of electrowetting on dielectric layers, Dahms (1969) measured the change in capillary rise of an electrolyte in a thin polyethylene tube as a function of the voltage applied across the tube wall. He showed that the presence of surface-active alcohols, which adsorb on the solid, greatly reduces the variation in $\gamma_{ls}$ with increasing voltage. Chudleigh (1976) was interested in the charge transfer from an electrolyte droplet to a thin polymer foil under high electric fields as a means of information storage and measured a reduction in the contact angle with applied voltage for different electrolytes. Vallet et al. (1996, 1999) conducted a number of experiments with sessile droplets of water or aqueous polymer solutions on thin (12–50 $\mu$m) polymer films. A voltage was applied between a small wire inserted into the droplet and a counter electrode beneath the insulating layer, as sketched in Figure 6*a*. For low voltages it was found that $\cos\theta(V) = \cos\theta(V=0) + \epsilon_0\epsilon_r V^2/(2d\gamma_{lv})$, where $d$ is the insulator layer thickness, $\epsilon_0$ is the permittivity of vacuum, and $\epsilon_r$ is the relative permittivity of the dielectric layer. Figure 6*b*,*c* illustrates that an applied potential decreases the contact angle. Above a critical voltage, the contact angle saturated at a fixed value; further increases in $V$ produced ionization phenomena manifest by light emission at the contact line (Figure 6*e*). Vallet et al. (1996) observed the ejection of fine droplets along the contact line of pure water at sufficiently high fields, and from a

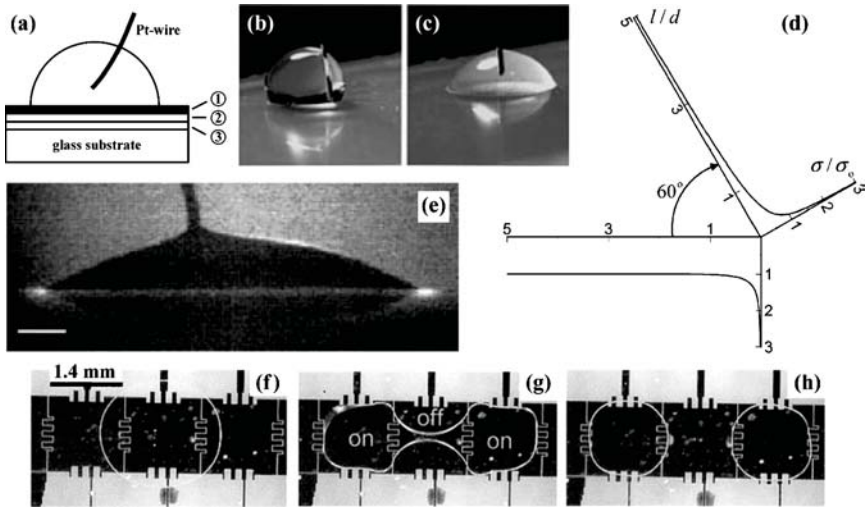


**Figure 6** (*a–c*) 0.1 mM $KNO_3$ sessile droplet with Pt wire on substrate consisting of (*1*) a hydrophobic layer of Teflon AF1600, (*2*) an electrically insulating layer (Parylene C or polyimide), and (*3*) an indium-tin-oxide counter-electrode. Applied voltage is (*b*) 0 and (*c*) 200 V. [Reprinted with permission from Welters & Fokkink (1998). Copyright Am. Chem. Soc.] (*d*) Computed surface charge density, $\sigma$, of a perfectly conducting liquid wedge with $\theta = 60^\circ$. [Reprinted with permission from Kang (2002). Copyright Am. Chem. Soc.] (*e*) Side view of a droplet on a 50 $\mu$m thick PTFE film at a voltage of 950 V (marker length 1 mm). The luminescence originating near the contact line is attributed to air ionization. Spectroscopic measurements show that the luminescence wavelength depends on the gas composition of the atmosphere and occurs in bursts of less than 100 ns duration. [Reprinted with permission from Vallet et al. (1999).] (*f–h*) Splitting of a droplet sandwiched between an electrode array and a transparent cover plate by electrowetting (applied voltage 25 V, gap size 70 $\mu$m, drop volume 0.2 $\mu$l). [Reprinted with permission from Cho et al. (2003). Copyright IEEE.]

simplified linear stability analysis (Vallet et al. 1999) concluded that the maximally unstable wavelength is roughly proportional to the thickness of the dielectric layer.

Thinner (of order 100 nm), pinhole-free insulator layers with a high dielectric breakdown field allow a reduction in the driving voltage (20–80 V) required for a significant modulation in contact angle. Arrays of individually addressable electrodes enable spatial modulation of contact angles $\theta_s(x)$. As discussed in section 4.1, contact angle gradients can be used to drive droplets with speeds on the order of 3–25 cm/s, and also be used to split (Figure 6*f–h*), merge, or mix droplets with very low power consumption (Cho et al. 2003, Pollack et al. 2000). The rapid change in droplet shapes induced by electrowetting has been utilized for tunable optical lenses (Berge & Peseux 2000), switchable mirrors (Lea 1986), and optical displays (Roques-Carmes et al. 2004). Electrowetting in combination

with superhydrophobic surfaces allows for even greater variability in contact angle (Krupenkin et al. 2004). To our knowledge, there are no hydrodynamic models describing droplet propulsion by electrowetting.

Several groups have attempted to explain the origin of the change in contact angle with applied potential using thermodynamic and electromechanical considerations. Following the derivation of Vallet et al. (1999), Kang (2002) considered a perfectly conducting droplet at constant potential $V$ resting on a thin dielectric layer of thickness $d$ deposited on a grounded electrode. He assumed the droplet profile in the vicinity of the contact line was a wedge with contact angle $\theta = (1 - p/q)\pi$, where $p$ and $q$ are positive integers. Solution of Laplace's equation, $\nabla^2\phi = 0$, for a conducting wedge leads to a surface charge density $\sigma$ that diverges at the contact line according to $|\sigma/\sigma_0| \sim (d/l)^\beta$, where $l$ is the distance from the contact line, $\sigma_0 = \epsilon_0 V/d$, $\beta = \alpha/(\alpha+1)$, and $\alpha = p/q$ (see Figure 6*d*). The corresponding divergence in the electric field is believed to cause air ionization and saturation of the contact angle at high fields (Figure 6*e*).

Instead of assuming that the droplet profile can be approximated by a solid wedge, Buehrle et al. (2003) balanced the electrical normal stress, $\epsilon_0 E^2/2$, at the air-liquid interface with the capillary pressure for a perfectly conducting droplet. They assumed that the surface slope far from the contact line was given by $\theta(V)$, as defined above. Numerical results based on energy minimization calculations show that the contact angle at the solid surface is equal to $\theta(V = 0)$, i.e., the Young-Dupré angle. Moreover, there develops a weak singularity in the droplet curvature at the contact line, which is reflected in the divergence of the surface charge density. Interestingly, Chou (2001) realized that a proper balance in the normal stress requires both the electrostatic and capillary contribution, but he concluded that the wedge approximation suffices on length scales smaller than the Debye screening length $\kappa^{-1}$. Kang et al. (2003) recently included double-layer effects and balanced the Maxwell stress and osmotic pressure in an electrolyte droplet disregarding the contribution from the capillary pressure. A complete description for an electrolyte droplet on an insulating layer subject to an external potential, including the effects of electrical double layers, Maxwell stresses, disjoining pressure, and capillary pressure, is still lacking. Such a description introduces at least two length scales, $d$ and $\kappa^{-1}$, which can be of comparable magnitude.

## 5. ACTUATION BY SURFACE SHEAR STRESSES

Gradients in the interfacial tension of a fluid-fluid interface (e.g., $\nabla\gamma_{lv}$) develop in the presence of nonuniformities in the surface temperature (thermocapillary flows), chemical composition (Marangoni flows), or charge density (electrocapillary flows). These give rise to a surface shear stress, $\tau$, which drives flow toward regions of higher interfacial tension. The interfacial shape and velocity profile is determined by the coupling of the Navier-Stokes (NS) equations with the equations for heat, mass, and charge transfer. For microscale flows with small geometric

aspect ratio and small Re and Bo numbers, the Peclet and Biot numbers also tend to be small and thermal variations across the film thickness are negligible. The NS equations and heat transfer equation then decouple and the flow profiles or shapes are simply determined from the thermal distribution applied to the substrate. This decoupling is generally not possible for Marangoni flows arising from compositional or charge nonuniformities because the local surfactant or surface charge concentration is coupled to the flow speed. The NS equations must be solved simultaneously with the convective-diffusive equation for surfactant transport along the interface and in the bulk phase, an equation of state relating the surface tension to the surface concentration, and an adsorption-desorption equation describing mass exchange between the interface and bulk fluids. For this reason, problems involving the transfer of neutral or charged surface-active species are much more difficult to analyze and control.

## 5.1. Microfluidic Streaming by Thermocapillary Stress

In experiments on Bénard convection, Volkoviski (1935) first observed that liquid films tend to spread toward the cooler side of a substrate. Hershey (1939) discussed how variations in surface tension generated by evaporation of a volatile mixture caused similar liquid migration. He designed a controlled experiment to monitor the spatial variation in film height caused by a prescribed variation in temperature along a thin film. Within the lubrication limit and neglecting capillary pressure, he derived the velocity profile corresponding to the balance of thermocapillary and hydrostatic forces under steady conditions, namely $\mu \mathbf{v} = z\nabla\gamma_{lv} + \rho g(z^2/2 - hz)\nabla h$, where $z = h(x)$ defines the position of the air-liquid interface. For a shallow pool of liquid, the corresponding film shape, $h(x)$, satisfies the equation $3\gamma_{lv} - \rho g h^2 = const.$ Hershey estimated that the cooler side of a horizontal water film 200 $\mu$m in thickness and subject to a temperature difference $\Delta T = 1^\circ$C (corresponding to $\Delta\gamma_{lv} = 0.15$ mN/m), would be elevated by 90 $\mu$m. For most liquids $\partial\gamma_{lv}/\partial T < 0$, although there exist interesting exceptions (Glinski et al. 1993). Ludviksson & Lightfoot (1971) were interested in explaining the origin of so-called supermeniscus films, i.e., film climbing beyond the equilibrium capillary length. They examined the spontaneous spreading of thin, nonvolatile films on a vertical wettable substrate subject to a linear temperature decrease (i.e., constant thermocapillary stress $\tau = \partial\gamma_{lv}/\partial T \cdot \nabla T$). Their interferometric profiles for the film shape and speed were compared with a simplified lubrication analysis (capillary pressure and contact line effects excluded). The average flow speed up the plate was computed to be $U = h\tau/(2\mu) - \rho g h^2/(3\mu)$, in good agreement with experiments.

The capability of guiding thermocapillary flow by chemical surface patterning provides a powerful method for controlled fluidic delivery. Thermal gradients can be generated by means of substrate embedded microheaters or by radiative heating from above (Hitt & Smith 1993, Schatz et al. 2002). Darhuber et al. (2003a) examined the horizontal thermocapillary spreading of Newtonian liquids emanating from a small reservoir pad onto a wettable microstripe subject to a linear

temperature decrease. The dimensionless equation for the maximum (centerline) film thickness is given by

$$\frac{\partial h}{\partial t} + \frac{\partial}{\partial \xi}\left(\frac{h^2}{\mu}\right) - \frac{192}{35} N_D \frac{\partial}{\partial \xi}\left(\frac{h^3}{\mu}\frac{\partial(\gamma h)}{\partial \xi}\right) + \frac{64}{105}\frac{\partial}{\partial \xi}\left[\frac{h^3}{\mu}\frac{\partial}{\partial \xi}\left(\gamma \frac{\partial^2 h}{\partial \xi^2}\right)\right] = 0, \tag{3}$$

where $\gamma(\xi)$ and $\mu(\xi)$ are the position-dependent surface tension and viscosity. The second term represents the longitudinal ($\hat{\xi}$-axis) flux due to the thermocapillary force; the third and fourth terms represent smaller flux contributions arising from the interfacial curvature along the transverse (for a parabolic cross-sectional shape, as in section 3.3) and longitudinal axes. Here, the dimensionless streamwise and transverse coordinates are scaled by $\ell = h_0(3\mathsf{Ca})^{-1/3}$ (Troian et al. 1989) and $w$, respectively, where $\mathsf{Ca} = \mu_0 U_0/\gamma_0$, $U_0 = 2h_0\tau/5\mu_0$, and the subscript 0 specifies parameter values at the stripe inlet position $\xi = 0$. The remaining parameter, $N_D = (\ell/w)^2$, signifies the competition between the dynamic length scale, $\ell$, which determines the longitudinal extent of capillary deformation near the moving front for an infinitely wide film, and the pattern feature size $w$. Experimental measurements for a wide parameter range show excellent agreement with numerical solutions of Equation 3 (Darhuber et al. 2003a). In the limit $N_D \to 0$ (i.e., chemically homogeneous surface), thermocapillary-spreading films undergo a fingering instability caused by the formation of a capillary ridge at the advancing front. This ridge is linearly unstable and produces the characteristic patterns shown in Figure 7*m–p*, where the wavelength $\lambda \sim \ell$ (Troian et al. 1989). Analyses of the rate of energy dissipation show that the fingering is caused by a combination of the higher flow mobility at the tips and a Rayleigh-type instability associated with the large curvature of the capillary ridge (Kataoka & Troian 1997, Spaid & Homsy 1996). For spreading on patterned surfaces, no such instability will occur provided $w < \lambda$ (Kataoka & Troian 1999).

Thermocapillary streaming therefore provides a reliable method of flow control that can also be used to convect small particles or biological material. For technological applications, an appealing feature of this transport method is that the driving force only depends on differences and not the absolute value of the applied temperature. Evaporation of the liquid film or thermal damage to biological material can be minimized by reducing the overall operating temperature.

## 5.2. Thermal Actuation of Droplets on Solid Surfaces

The propulsion of small droplets by thermocapillary forces necessitates a partially wetting surface to prevent the formation of precursor (de Gennes 1985) or trailing films that can cause cross-contamination. The number of available surface treatments for converting wettable to partially wettable substrates that are smooth and homogeneous (to avoid hysteresis) is somewhat limited. Nonetheless, a number of groups have examined droplet migration by thermocapillary forces both experimentally and theoretically (Brochard 1989; Brzoska et al. 1993; Chen et al.

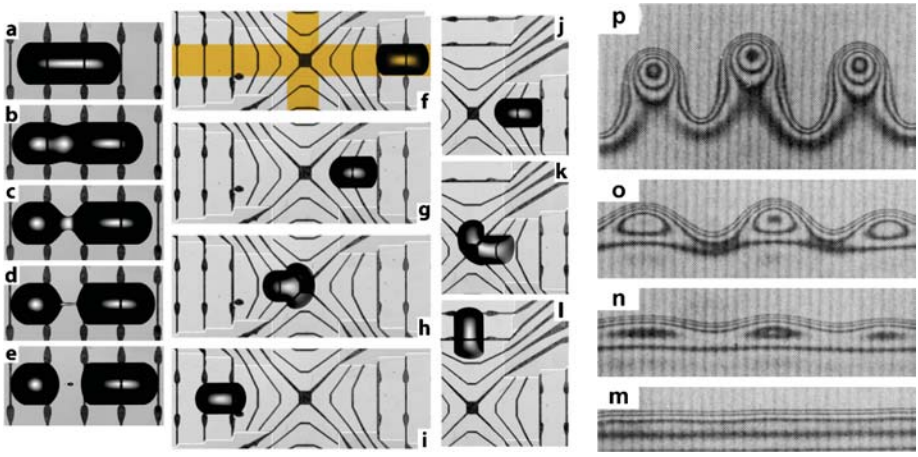


**Figure 7** (*a–e*) Image sequence showing the thermocapillary splitting of a dodecane droplet on a partially wetting stripe ($w = 1000\,\mu$m, $\Delta t_{\text{total}} = 8.5$ s). The voltage applied to the embedded microheaters (electrical resistance 155 Ω) was 2.5 V (Darhuber et al. 2003b). (*f–i*) Image sequence of dodecane droplet propelled by thermocapillary forces. Intersecting orange stripes designate partially wetting regions ($w = 1000\,\mu$m, $\Delta t_{\text{total}} = 104$ s) (Darhuber et al. 2003b). (*j–l*) Dodecane droplet turning a 90° corner ($\Delta t_{\text{total}} = 164$ s) (Darhuber et al. 2003b). (*m–p*) Evolution of fingering instability at the leading edge of a silicone oil film advancing on a chemically homogeneous substrate (silicon wafer) due to thermocapillary forces (applied shear stress $\tau = 0.18$ Pa, $\Delta t_{\text{total}} = 17$ min, instability wavelength $\lambda \approx 500\,\mu$m) (Cazabat et al. 1990).

2004; Darhuber et al. 2003b,c; Ford & Nadim 1994; Smith 1995; Yarin et al. 2002). Brochard (1989) studied the migration of 2D droplets driven by a small thermal gradient. A similar force balance as used for chemically graduated surfaces (section 4.1) was used to describe droplet motion subject to spatial variations in $\gamma_{lv}$, $\gamma_{ls}$, and $\gamma_{sv}$. Depending on the relative strength of the driving forces at each interface, the droplet can move toward or away from the cooler end of the substrate. When contact angle hysteresis is explicitly incorporated into the model (Brzoska et al. 1993), droplet motion is only possible above a critical droplet radius (neglecting thermal variations in $\gamma_{sv}$ and $\gamma_{ls}$) for a given thermocapillary stress. Above this critical value, the flow speed increases linearly with the droplet radius $R$ and applied thermal gradient $\nabla T$. These predictions were confirmed by experiments with silicone oil droplets ($2 \lesssim R \lesssim 10$ mm) moving on a hexadecyltrichlorosilane-coated silicon wafer ($11 \lesssim \theta_s \lesssim 13^\circ$) subject to $|\nabla T| < 1^\circ$C/mm. In their model Ford & Nadim (1994) relieved the stress singularity at the contact line by incorporating a Navier slip condition and examined larger thermal gradients by allowing surface deformation beyond a cylindrical cap. The droplet speed then depends on the Navier slip coefficient, which is exceedingly difficult to measure experimentally. Smith (1995) conducted a full hydrodynamic analysis in the lubrication limit for

a 2D droplet subject to a constant thermocapillary stress. He assumed the speed of the contact lines depended on the contact angles according to $v_{cl} = K(\theta - \theta_A)^3$ and $v_{cl} = K(\theta_R - \theta)^3$ and used a Navier slip condition at the liquid-solid boundary. His steady-state solutions exhibit thermocapillary recirculation within the droplet, which influence the advancing and receding contact angles. Yarin et al. (2002) examined the thermocapillary migration of axisymmetric alkane droplets clinging to a partially wettable cylindrical fiber. Experimental results for droplet position as a function of time were compared with a simplified model that neglects capillary pressure and contact angle hysteresis but includes the variation of viscosity with temperature, an effect not included in the previous models. Chen et al. (2004) recently measured the depinning force and minimum droplet radius required for droplet mobilization on partially wetting surfaces, as well as the dependence of the droplet speed on radius, thermal gradient, and liquid material parameters. The results are in good agreement with Ford & Nadim's (1994) model for nonconstant thermocapillary stress.

Higher droplet speeds and better directional control can be achieved by combining thermocapillary propulsion with chemically defined pathways and large but localized thermal gradients. Darhuber et al. (2003b,c) recently used electronically addressable microheater arrays embedded within a glass substrate to propel droplets of various liquids (including water) along a network of partially wettable microstripes (see Figure 7). Such active control allows different thermal distributions to be activated on demand for various fluidic manipulations. Sequential activation of microheaters is used for droplet transport from one location to another as shown in Figure 7*f–l*. Application of a sawtooth-like temperature profile will split a droplet (Figure 7*a–e*) or rivulet into a sequence of smaller droplets due to film rupture at the hot spots. The same principle can be used to trap or release liquid drops from a cold spot or to trigger or quench site-specific chemical reactions. Addressable heating arrays can also be used to apply combinations of streamwise and transverse thermal gradients for efficient mixing in microscale geometries. Darhuber et al. (2004) also examined convective mass transfer in thermocapillary flows on patterned substrates. Three important mixing regimes, based on analogues of purely diffusive dynamics, Rhines-Young shear-augmented diffusion, and Taylor-Aris dispersion, were investigated for possible use in microscale devices.

## 5.3. Flow Actuation by Marangoni Stresses

In contrast to thermocapillary propulsion, it is much more difficult to manipulate droplet motion on a solid substrate by varying the surface chemical composition of the liquid film. Small droplets, however, can be "actively" propelled within a liquid film or bulk liquid phase. In this section, we briefly review the mechanisms governing Marangoni-driven transport along with some experimental demonstrations. "Passive" flow retardation effects or shape deformations accompanying surfactant transport and adsorption at interfaces in drops or bubbles are not discussed.

Quincke (1888) conducted experiments involving the migration and oscillation of air bubbles in a layer of distilled water held between two horizontal glass plates. Releasing a stream of alcohol with a flow rate of a few $cm^3$/hr near a large 2-cm gas bubble caused the bubble to move toward the alcohol source and to oscillate with a period of 1–3 s. Higher flow rates induced higher oscillation frequencies. By momentum conservation, the Marangoni stress that is directed toward the region of higher surface tension (less alcohol) causes the bubble to migrate toward the opposite end (alcohol enriched). Droplet propulsion can also be achieved by proximity to a film of lower surface tension. Figure 8*a–d* shows an example of a droplet of hexadecane ($\gamma_{lv} = 27.0\,m$N/m) deposited near a miscible film of polydimethylsiloxane (PDMS; $\gamma_{lv} = 20.0\,m$N/m) on a partially wettable silicon wafer. As the spreading PDMS film approaches the hexadecane, the droplet is propelled forward by a Marangoni stress. Karlsson et al. (2002) reported Marangoni-induced flow through a lipid bilayer nanotube (diameter 100–300 nm) connecting two surface-immobilized lipid bilayer vesicles (diameter 5–25 $\mu$m). Mechanical deformation of one vesicle from a spherical to ellipsoidal shape (characterized by a higher surface to volume ratio and increased membrane tension) induces flow of lipid molecules from the undeformed to the deformed vesicle through the nanotube interior (see Figure 8).

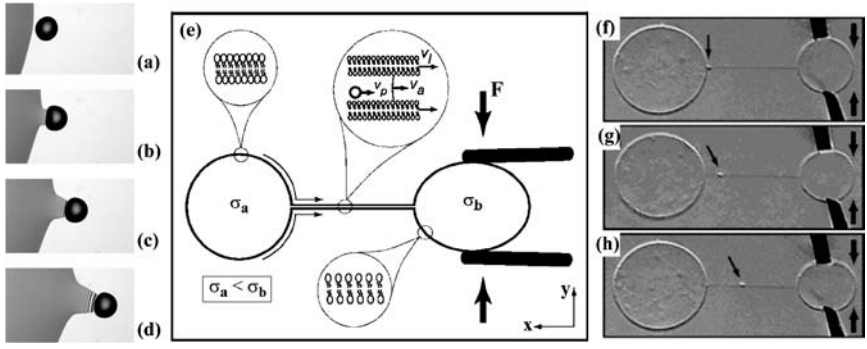


**Figure 8** (*a–d*) Propulsion of a droplet of hexadecane (volatile, $\gamma_{lv} = 27.0\,m$N/m, $\mu = 3.0\,m$Pa s) by a spreading film of PDMS (nonvolatile, $\gamma_{lv} = 20.0\,m$N/m, $\mu = 20\,m$Pa s) on a dodecyltrichlorosilane-coated silicon wafer. Optical interference images (width 2 mm) recorded at $t = 0$, 8, 24, and 60 s (Darhuber & Troian, unpublished). (*e*) Schematic illustration of two substrate-immobilized lipid bilayer vesicles (diameter 5 – 25 $\mu$m) with surface tension $\sigma_a < \sigma_b$ connected by a lipid bilayer nanotube (diameter 100 – 300 nm). Two carbon fibers are used to deform vesicle 'b' into an ellipsoidal shape causing an increase in the vesicle's surface tension, which is presumed to induce Marangoni-driven flow of lipid restoring the system to equilibrium. (*f–h*) Image sequence showing transport of a small liposome (position denoted by black arrow) within a lipid bilayer nanotube of length 32 $\mu$m. [Reprinted with permission from Karlsson et al. (2002). Copyright Am. Chem. Soc.]

In microfluidic applications, surface tension gradients can spontaneously arise, for example, during droplet splitting or coalescence, mixing of samples, or chemical reactions. Typically, the gradients generated during contact of dissimilar liquids are much larger than corresponding thermocapillary variations. Deposition of biological liquids, which often contain surface-active material, onto a liquid film with higher $\gamma_{lv}$ will generate Marangoni stresses that can cause rapid film thinning and rupture. It is therefore important to understand the basic phenomena governing this class of flows.

Levich (1941) outlined the thermodynamic basis for the shear stress condition at an interface containing surface-active molecules, which reduce the surface tension in proportion to the local concentration. In addition to capillary pressure, there can develop a tangential stress $\tau = \nabla_s \gamma_{lv} = (d\gamma_{lv}/d\Gamma) \cdot \nabla_s \Gamma$. The surfactant surface concentration, $\Gamma(\mathbf{x}, t)$, is governed by the equation (Scriven 1960)

$$\frac{\partial \Gamma}{\partial t} + \nabla_s \cdot (\Gamma \mathbf{u}_s) + \Gamma(\nabla_s \cdot \mathbf{n})(\mathbf{u} \cdot \mathbf{n}) = D_s \nabla_s{}^2 \Gamma. \quad (4)$$

The surfactant flux depends on the tangential component of the surface velocity, $\mathbf{u}_s = (\mathbf{I} - \mathbf{nn}) \cdot \mathbf{u}$, the mean curvature of the interface, $\nabla_s \cdot \mathbf{n}$, and the surfactant (surface) diffusion coefficient $D_s$. Soluble surfactants require specification of the interfacial adsorption/desorption kinetics relating the surface concentration $\Gamma$ to the bulk (B) concentration $c$, thereby coupling Equation 4 to the bulk convection-diffusion equation $\partial c/\partial t + \mathbf{u} \cdot \nabla c = D_B \nabla^2 c$. For thin film flows on a flat substrate, the variation in liquid thickness is determined from

$$\frac{\partial h}{\partial t} - \nabla \cdot \left( \frac{h^3}{3\mu} \nabla p - \frac{h^2}{2\mu} \nabla \gamma_{lv} \right) = 0. \quad (5)$$

Equations 4 and 5 are coupled through the dependence of the surface tension on surfactant concentration, $\gamma_{lv}[\Gamma]$, and the surface velocity $\mathbf{u}_s = h\nabla\gamma_{lv}/\mu - h^2\nabla p/(2\mu)$.

Active control over the speed of droplets or solid particles convected within a thin liquid film can be enforced by electrochemical modulation of $\nabla_s \gamma_{lv}$. A voltage applied between two electrodes positioned near opposite ends of a thin aqueous film was used to modulate $\gamma_{lv}$ by tuning the active state of soluble surfactants with redox-active head groups (Figure 9*b*). A droplet of a nematic liquid crystal was convected along a 1 mm deep aqueous film of $Fc(CH_2)_{11}-N^+(CH_3)_3Br^-$ by applying a voltage difference of 0.6 V (Gallardo et al. 1999). Speeds of 4 mm/s were achieved with $\Delta\gamma_{lv} = 22$ mN/m.

Equally large changes in the dynamic surface tension of liquids are possible by UV exposure of aqueous solutions containing photosensitive surfactants. As shown in Figure 9*c*,*d*, active release of droplets from a pendant array is triggered by selective exposure of droplets to UV light. This release is not caused by Marangoni effects but by the sharp reduction in surface tension upon UV exposure, which causes the Bond number, $\rho g R^2/\gamma_{lv}$, to increase above the critical value for drop detachment. Spatial modulation of the illumination intensity, however, could

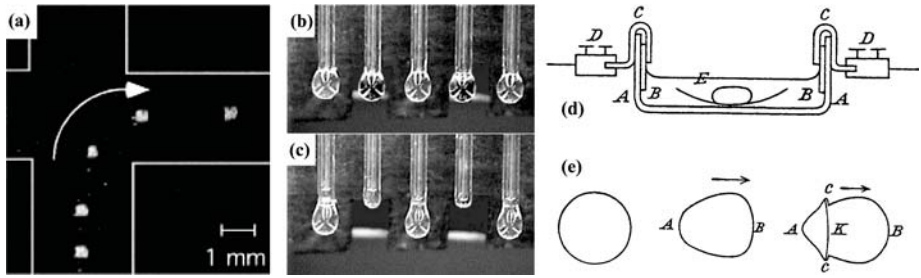


**Figure 9** (*a*) Time-lapse image ($\Delta t = 2$ s) of a liquid crystal droplet convected by an aqueous film containing an electroactive surfactant. A potential difference of 0.6 V was applied to Pt electrodes at the south and east ends of the trajectory shown. [Reprinted with permission from Gallardo et al. (1999). Copyright AAAS.] (*b*,*c*) Light-activated capillary release of droplets of an aqueous (0.1 M NaCl, 0.16 mM SDS) solution of a photosensitive azobenzene surfactant. (*b*) An array of five pendant droplets formed at the tips of glass capillaries. (*c*) After illumination with UV light, the surface tension of two drops becomes too low to support the drop weight. [Reprinted with permission from Shin & Abbott (1999). Copyright Am. Chem. Soc.] (*d*,*e*) Experimental setup for electrocapillary propulsion of Hg droplets. Copper clamps (*C*) are used to suspend two platinum electrodes (*B*) into 45 $cm^3$ of a 10 mM $KNO_3$ solution in a 10 cm long glass container (*A*). A watch glass (*E*) contains the droplet of mercury of initial diameter 11 mm. (*e*) Droplet shapes corresponding to electric currents of 0, 10, and 20 mA (Christiansen 1903).

provide actively tunable Marangoni stresses as a function of position and time. Such concepts can be extended to droplet actuation or propulsion of floating particles in analogy to techniques described in section 4.1.

## 5.4. Electrocapillary and Electrochemical Marangoni Flows

Chemical reactions at interfaces can generate variations in interfacial tension although these phenomena are also difficult to control. Paalzow (1858) and Bernstein (1900) describe the irregular motion and oscillations of a mercury droplet in an acidic electrolyte in proximity to a dissolving potassium dichromate crystal. In one experiment Bernstein (1900) centered a small mercury droplet inside a glass capillary filled with dilute sulfuric acid. When the diffusing front of $Cr_2O_7^{2-}$ ions from a small $Cr_2O_7K_2$ crystal positioned at one end of the capillary reached the center of the tube, the mercury drop moved toward the crystal. The motion was attributed to the reduction and spatial inhomogeneity in $\gamma_{Hg,el}$ due to oxidation of the mercury by the diffusing ions. Homogenizing the ion concentration by stirring caused any motion or oscillation of the mercury drop to cease. Bernstein's interest in this system was fuelled by what he thought was a striking analogy between the drop migration in a concentration gradient and the locomotion of primitive organisms. He presented a simple theoretical model for motion caused by variations in the capillary pressure and contact angles of mercury on the glass surface but

neglected Marangoni stresses. Propulsion methods such as these, however, remain largely unexplored for fluidic applications.

The phenomena described in section 4.2.1 result from electrically generated normal stresses that modify the equilibrium conformation of sessile electrolyte droplets. External electric fields, however, can generate both normal and tangential stresses, which cause variations in the interfacial tension at a fluid-fluid boundary, thereby generating flow. Erman (1809) and Christiansen (1903) first described the migration of a mercury drop in an electrolyte subject to an electric field. Figure 9*d*,*e* shows Christiansen's experimental setup and the significant distortion in droplet shape observed with increasing electrical current. Levich (1962) presented a first-order model for the migration velocity of an ideally polarizable, spherical liquid metal droplet of radius $R$ in a weak electric field $E$. The droplet speed was estimated to be $U = \sigma ER/(2\mu_{el} + 3\mu_{Hg} + \sigma^2/\kappa_{el})$, where $\mu_{el}$ and $\mu_{Hg}$ are the viscosities of the electrolyte and liquid metal and $\kappa_{el}$ is the electrolyte conductivity. This velocity is orders of magnitude larger than typical speeds for electrophoretic actuation of solid particles. For a solid particle, the viscous motion of the liquid decays within the electrical double layer of thickness, $d$, whereas for a liquid metal droplet, the velocity field persists over a distance comparable to the droplet radius $R$, leading to a mobility increase by a factor of $R/d$. This propulsion method is not limited to mercury droplets in electrolytes. The speed of an emulsion droplet of conductivity $\kappa_{em}$ can be derived in similar fashion to give $U = \sigma ER/[2\mu_{el} + 3\mu_{em} + \sigma^2(1/\kappa_{el} + 2/\kappa_{em})] \approx \kappa_{em} ER/\sigma$, where the approximation holds for a small emulsion conductivity $\kappa_{em}$. Beni et al. (1982) constructed a ("continuous electrowetting") system based on mercury/electrolyte actuation capable of generating droplet speeds on the order of 10 cm/s using only 1 V.

## 6. CLOSING REMARKS

Microfluidics is not a unified field, but rather one where diverse applications demand diverse solutions. This article describes a number of methods available for fluidic manipulation and control of free surface flows on uniform or textured surfaces by application of normal and shear stresses. As the surface to volume ratio increases, the dynamics of droplets and thin liquid films constitutes a class of moving boundary flows increasingly sensitive to boundary effects and surface forces. The boundary phenomena associated with movement of the contact line (contact angle hysteresis, dynamic contact angles, disjoining pressure, line tension, and slip), need to be resolved at the molecular level and incorporated into continuum hydrodynamic models. Currently, "hybrid" approaches are being examined as a way of coupling molecular dynamics and Navier-Stokes simulations to provide an accurate description of surface effects from micro- to mesoscopic length scales (O'Connell & Thompson 1995, Nie et al. 2004).

Experimental investigation of the molecular behavior requires metrology methods suited to smaller length scales. Many high-resolution tools for surface science

require vacuum conditions, which are incompatible with the presence of almost any liquid. Existing metrology techniques are better adapted to the investigation of thin films, rather than to small-scale structures of high-aspect ratio. The reduced interaction volumes also significantly decrease signal levels. These experimental difficulties will necessitate development and adaption of high-resolution techniques for probing the conformation and dynamics of liquids on patterned surfaces.

For these reasons, the field of microfluidics is among the fastest-growing areas in fluid mechanics. The synergy created by the confluence of microfabrication, hydrodynamics, and physical chemistry offers exciting opportunities for scientific progress across multiple disciplines.



## ACKNOWLEDGMENTS

The authors are very grateful for financial support from the National Science Foundation, Unilever Research U.S., NASA, and the U.S. Army.

# APPENDIX

## Dip-Coating of Chemically Patterned Substrates

The deposition of a liquid film on a chemically patterned surface can be achieved by withdrawing the substrate from a liquid reservoir at constant speed. For small Ca, withdrawal of a substrate containing a wettable microstripe entrains a liquid film

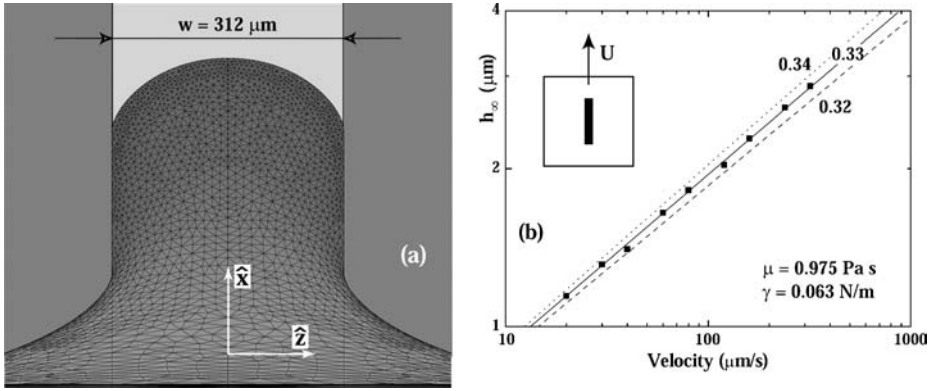


**Figure 10** (*a*) Surface Evolver simulation of equilibrium capillary rise height for glycerol on a hydrophilic stripe ($\theta_{\text{int}} = 5^\circ$ and $w = 312\,\mu$m) patterned on a hydrophobic substrate ($\theta_{\text{ext}} = 95^\circ$) (Darhuber et al. 2000b). (*b*) Measurements of the entrained film thickness, $h_\infty$, versus the vertical withdrawal speed, $U$, on an isolated hydrophilic stripe (dimensions $49\,\mu\text{m} \times 4\,\text{mm}$) from a glycerol reservoir (Darhuber et al. 2000b).

whose thickness is typically in the micron range (Darhuber et al. 2000b). Neglecting gravitational drainage, the equation governing the dimensionless centerline height, $\bar{h}(\bar{x})$, of the liquid ribbon is given by

$$\bar{h}^3\left[\left(\frac{w}{x_s}\right)^2\frac{\partial^3\bar{h}}{\partial\bar{x}^3}+\frac{\partial^3\bar{h}}{\partial\bar{x}\partial\bar{z}^2}\right]=3\mathsf{K}\mathrm{Ca}\frac{x_s w^2}{h_\infty^3}(1-\bar{h}). \quad (6)$$

Here, $\mathsf{K}$ is a constant of order one, $h_\infty$ is the entrained thickness far from the reservoir, $w$ is the width of the wettable stripe, and $x_s$ represents the characteristic streamwise length scale. This length scale, which decreases linearly with $w$, is set by the radius of curvature in the static meniscus region (since $\mathrm{Ca} \ll 1$) or equivalently by the equilibrium height of capillary rise for a liquid on a wettable microstripe (Figure 10*a*). The streamwise and lateral coordinates are therefore scaled by $x_s$ and $w$, respectively. For $x_s \sim w$, the right-hand term of Equation 6 yields the dynamic scaling $h_\infty \sim w\mathrm{Ca}^{1/3}$. This equation differs considerably from the expression for film entrainment on homogeneous substrates, $h_\infty \sim \ell_c\mathrm{Ca}^{2/3}$ (Derjaguin 1943, Landau & Levich 1942), and predicts the formation of very thin liquid ribbons. Experimental data confirm the reduced entrainment exponent 1/3 (Figure 10*b*) as well as the linear dependence on stripe width (Darhuber et al. 2000b). Liquid deposition on chemically patterned substrates has been used to fabricate microlens and colloidal arrays (Biebuyck & Whitesides 1994, Xia et al. 2003).

**The *Annual Review of Fluid Mechanics* is online at http://fluid.annualreviews.org**

## LITERATURE CITED


Adamson AW. 1990. *Physical Chemistry of Surfaces*. New York: John Wiley & Sons

Bain CD, Burnett-Hall GD, Montgomerie RR. 1994. Rapid motion of liquid drops. *Nature* 372:414–15

Barrat JL, Bocquet L. 1999. Influence of wetting properties on hydrodynamic boundary conditions at a fluid/solid interface. *Faraday Discuss.* 112:119–27

Bart SF, Tavrow LS, Mehregany M, Lang JH. 1990. Microfabricated electrohydrodynamic pumps. *Sens. Actuators* A21:193–97

Bell JM, Cameron FK. 1906. The flow of liquids through capillary spaces. *J. Phys. Chem.* 10:658–74

Beni G, Hackwood S, Jackel JL. 1982. Continuous electrowetting effect. *Appl. Phys. Lett.* 40:912–14

Berge B, Peseux J. 2000. Variable focal lens controlled by an external voltage: an application of electrowetting. *Eur. Phys. J.* E3:159–63

Bernstein J. 1900. Chemotropische Bewegung eines Quecksilbertropfens—Zur Theorie der amöboiden Bewegung. *Archiv für Physiologie* 80:628–37

Bico J, Quéré D. 2002. Self-propelling slugs. *J. Fluid Mech.* 467:101–27

Biebuyck HA, Whitesides GM. 1994. Self-organization of organic liquids on patterned self-assembled monolayers of alkanethiolates on gold. *Langmuir* 10:2790–93

Billet DF, Hough DB, Ottewil RH. 1976. Studies on the contact angle of the charged silver iodide-solution-vapour interface. *J. Electroanal. Chem.* 74:107–20

Bouasse H. 1924. Capillarité, phénomènes superficiels. Paris: Delagrave

Brakke KA. 1992. The Surface Evolver. *Exp. Math.* 1:141–64

Brinkmann M, Lipowsky R. 2002. Wetting morphologies on substrates with striped surface domains. *J. Appl. Phys.* 92:4296–306

Brochard F. 1989. Motions of droplets on solid surfaces induced by chemical or thermal gradients. *Langmuir* 5:432–38

Brzoska JB, Brochard-Wyart F, Rondelez F. 1993. Motions of droplets on hydrophobic model surfaces induced by thermal gradients. *Langmuir* 9:2220–24

Buehrle J, Herminghaus S, Mugele F. 2003. Interface profiles near three-phase contact lines in electric fields. *Phys. Rev. Lett.* 91:086101–4

Burdon RS, Oliphant ML. 1927. The problem of the surface tension of mercury and the action of aqueous solutions on a mercury surface. *Transact. Faraday Soc.* 23:205–13

Busscher HJ, Stokroos I, van der Mei HC, Rouxhet PG, Schakenraad JM. 1992. Preparation and characterization of superhydrophobic FEP-teflon surfaces. *J. Adhes. Sci. Technol.* 6:347–56

Cassie ABD, Baxter S. 1944. Wettability of porous surfaces. *Trans. Farad. Soc.* 40:546–51

Cazabat AM, Heslot F, Troian SM, Carles P. 1990. Fingering instability of thin spreading films driven by temperature gradients. *Nature* 346:824–26

Chatelier RC, Drummond CJ, Chan DYC, Vasic ZR, Gengenbach TR, et al. 1995. Theory of contact angles and the free energy of formation of ionizable surfaces. *Langmuir* 11:4122–28

Chaudhury MK, Whitesides GM. 1992. How to make water run uphill. *Science* 256:1539–41

Chen JZ, Troian SM, Darhuber AA, Wagner S. 2005. Effect of contact angle hysteresis on thermocapillary droplet propulsion. *J. Appl. Phys.* In press

Chen YL, Helm CA, Israelachvili JN. 1991. Molecular mechanisms associated with adhesion and contact angle hysteresis of monolayer surfaces. *J. Phys. Chem.* 95:10736–47

Cho SK, Moon H, Kim CJ. 2003. Creating, transporting, cutting, and merging liquid droplets by electrowetting-based actuation for digital microfluidic circuits. *J. Microelectromech. Syst.* 12:70–80

Chou T. 2001. Geometry-dependent electrostatics near contact lines. *Phys. Rev. Lett.* 87:106101–4

Christiansen C. 1903. Kapillarelektrische Bewegungen. *Ann. Phys.* 12:1072–79

Chudleigh PW. 1976. Mechanism of charge transfer to a polymer surface by a conducting liquid contact. *J. Appl. Phys.* 47:4475–83

Concus P, Finn R. 1974. On capillary free surfaces in the absence of gravity. *Acta Math.* 132:177–98

Cox RG. 1986. The dynamics of the spreading of liquids on a solid surface. I. Viscous flow. *J. Fluid Mech.* 168:169–94

Cubaud T, Fermigier M. 2001. Faceted drops on heterogeneous surfaces. *Europhys. Lett.* 55:239–45

Dahms H. 1969. Electrocapillary measurements at the interface insulator-electrolytic solution. *J. Electrochem. Soc.* 116:1532–34

Daniel S, Chaudhury MK. 2002. Rectified motion of liquid drops on gradient surfaces induced by vibration. *Langmuir* 18:3404–7

Darhuber AA, Troian SM, Miller SM, Wagner S. 2000a. Morphology of liquid microstructures on chemically patterned surfaces. *J. Appl. Phys.* 87:7768–75

Darhuber AA, Troian SM, Davis JM, Miller SM, Wagner S. 2000b. Selective dip-coating of chemically micropatterned surfaces. *J. Appl. Phys.* 88:5119–26

Darhuber AA, Troian SM, Reisner WW. 2001a. Dynamics of capillary spreading along hydrophilic microstripes. *Phys. Rev. E* 64:031603:1–8

Darhuber AA, Davis JM, Troian SM, Reisner WW. 2003a. Thermocapillary actuation of liquid flow on chemically patterned surfaces. *Phys. Fluids* 15:1295–304

Darhuber AA, Valentino JP, Davis JM, Troian SM, Wagner S. 2003b. Microfluidic actuation by modulation of surface stresses. *Appl. Phys. Lett.* 82:657–59

Darhuber AA, Valentino JP, Troian SM, Wagner S. 2003c. Thermocapillary actuation of droplets on chemically patterned surfaces by programmable microheater arrays. *J. Microelectromech. Syst.* 12:873–79

Darhuber AA, Chen JZ, Davis JM, Troian SM. 2004. A study of mixing in thermocapillary flows on micropatterned surfaces. *Phil. Trans. R. Soc. London* A362:1037–58

Davis SH. 1980. Moving contact lines and rivulet instabilities. Part 1. The static rivulet. *J. Fluid Mech.* 98:225–42

de Gennes PG. 1985. Wetting: statics and dynamics. *Rev. Mod. Phys.* 57:827–63

Derjaguin B. 1943. Thickness of liquid layer adhering to walls of vessels on their emptying and the theory of photo- and motion picture film coating. *Dokl. Acad. Sci. URSS* 39:13–16

Dettre RH, Johnson RE. 1965. Contact angle hysteresis. IV. Contact angle measurements on heterogeneous surfaces. *J. Phys. Chem.* 69:1507–15

Digilov R. 2000. Charge-induced modification of contact angle: the secondary electrocapillary effect. *Langmuir* 16:6719–23

Dos Santos FD, Ondarçuhu T. 1995. Free-running droplets. *Phys. Rev. Lett.* 75:2972–75

Duffy DC, Gillis HL, Lin J, Sheppard NF, Kellogg GJ. 1999. Microfabricated centrifugal microfluidic systems. *Anal. Chem.* 71:4669–78

Dunn PD, Reay DA. 1978. *Heat Pipes.* Oxford: Pergamon Press

Dussan EB. 1976. The moving contact line: the slip boundary condition. *J. Fluid. Mech.* 77:665–84

Dussan EB. 1979. On the spreading of liquids on solid surfaces: static and dynamic contact lines. *Annu. Rev. Fluid Mech.* 11:371–400

Erman P. 1809. Wahrnehmungen über das gleichzeitige Entstehen von mechanischer Cohärenz und chemischer Verwandtschaft. *Ann. Phys.* 32:261–92

Faghri A, Juhasz AJ, Mahefkey T, eds. 1993. *Heat Pipes and Capillary Pumped Loops*. New York: ASME

Finn R. 1986. *Equilibrium Capillary Surfaces*. New York: Springer Verlag

Fokkink LGJ, Ralston J. 1989. Contact angles on charged surfaces. *Coll. Surf.* 36:69–76

Ford ML, Nadim A. 1994. Thermocapillary migration of an attached drop on a solid surface. *Phys. Fluids* 6:3183–85

Gallardo BS, Gupta VK, Eagerton FD, Jong LI, Craig VS, et al. 1999. Electrochemical principles for active control of liquids on submillimeter scales. *Science* 283:57–60

Gau H, Herminghaus S, Lenz P, Lipowsky R. 1999. Liquid morphologies on structured surfaces: from microchannels to microchips. *Science* 283:46–49

Gibbs JW. 1961. *Scientific Papers Vol. 1* , New York: Dover

Glinski J, Chavepeyer G, Platten JK, De Saedeleer C. 1993. Interfacial tension and interface phase transitions in two-phase water-long-chained alcohols systems. *J. Colloid Interface Sci.* 158:382–87

Greenspan HP. 1978. On the motion of a small viscous droplet that wets a surface. *J. Fluid. Mech.* 84:125–43

Hare EF, Zisman WA. 1955. Autophobic liquids and the properties of their adsorbed films. *J. Phys. Chem.* 59:335–40

Hauksbee F. 1712. An account of an experiment touching the direction of a drop of oil of oranges, between two glass planes, towards any side of them that is nearest press'd together. *Philosoph. Transact.* 27:395–96

Helmholtz HLF. 1882. *Wissenschaftliche Abhandlungen I*. Leipzig: Johann Ambrosius Barth. 925 pp.

Hershey AV. 1939. Ridges in a liquid surface due to the temperature dependence of surface tension. *Phys. Rev.* 56:204

Hitt DL, Smith MK. 1993. Radiation-driven thermocapillary flows in optically thick liquid films. *Phys. Fluids A* 5:2624–32

Huh C, Mason SG. 1977. Effects of surface roughness on wetting. *J. Colloid Interface Sci.* 60:11–38

Ichimura K, Oh SK, Nakagawa M. 2000. Light-driven motion of liquids on a photoresponsive surface. *Science* 288:1624–26

Ishihara K, Okazaki A, Negishi N, Shinohara I, Okano T, et al. 1982. Photo-induced change in wettability and binding ability of azoaromatic polymers. *J. Appl. Polym. Sci.* 27:239–45

Jang J, Lee SS. 2000. Theoretical and experimental study of magnetohydrodynamic micropump. *Sens. Actuators A* 80:84–89

Johnson RE, Dettre RH. 1964. Contact angle hysteresis. III. Study of an idealized heterogeneous surface. *J. Phys. Chem.* 68:1744–50

Jones TB, Gunji M, Washizu M, Feldman MJ. 2001. Dielectrophoretic liquid actuation and nanodroplet formation. *J. Appl. Phys.* 89:1441–48

Jones TB, Wang KL, Yao DJ. 2004. Frequency-dependent electromechanics of aqueous liquids: electrowetting and dielectrophoresis. *Langmuir* 20:2813–18

Kabanov B, Frumkin A. 1933. Über die Grösse elektrolytisch entwickelter Gasblasen. *Z. Phys. Chem.* A165:433–52

Kang KH. 2002. How electrostatic fields change contact angle in electrowetting. *Langmuir* 18:10318–22

Kang KH, Kang IS, Lee CM. 2003. Wetting tension due to Coulombic interaction in charge-related wetting phenomena. *Langmuir* 19:5407–12

Karlsson R, Karlsson M, Karlsson A, Cans AS, Bergenholtz J, et al. 2002. Moving-wall-driven flows in nanofluidic systems. *Langmuir* 18:4186–90

Kataoka DE, Troian SM. 1997. A theoretical study of instabilities at the advancing front of thermally driven coating films. *J. Colloid Interface Sci.* 192:350–62

Kataoka DE, Troian SM. 1999. Patterning liquid flow on the microscopic scale. *Nature* 402:794–97

Krotov VV, Rusanov AI. 1999. *Physicochemical Hydrodynamics of Capillary Systems*. London: Imperial College Press

Krupenkin TN, Taylor JA, Schneider TM, Yang S. 2004. From rolling ball to complete wetting: the dynamic tuning of liquids on nanostructured surfaces. *Langmuir* 20:3824–27

Kunugi Y, Nonaku T, Chong YB, Watanabe N. 1993. Preparation of ultrahydrophobic electrodes and their electrochemical properties. *J. Electroanalyt. Chem.* 353:209–15

Landau L, Levich B. 1942. Dragging of a liquid by a moving plate. *Acta Physicochim. URSS* 17:42–54

Langbein DW. 2002. *Capillary Surfaces*. Berlin: Springer Verlag

Laskowski J, Kitchener JA. 1969. The hydrophilic-hydrophobic transition on silica. *J. Colloid Interface Sci.* 29:670–79

Lau KKS, Bico J, Teo KBK, Chhowalla M, Amaratunga GAJ, et al. 2003. Superhydrophobic carbon nanotube forests. *Nano Lett.* 3:1701–5

Lea MC. 1986. Electrocapillary devices. *U.S. Patent No.* 4,583,824

Leal LG. 1992. *Laminar Flow and Convective Transport Processes*. Boston: Butterworth-Heinemann

Lee J, Kim CJ. 2000. Surface-tension-driven microactuation based on continuous electrowetting. *J. Microelectromech. Syst.* 9:171–80

Levich V. 1941. The damping of waves by surface-active substances I. *Acta Physicochim. URSS* 14:307–28

Levich VG. 1962. *Physicochemical Hydrodynamics*. Englewood Cliffs, NJ: Prentice Hall

Lippmann G. 1875. Relations entre les phènoménes électriques et capillaires. *Ann. Chim. Phys.* 5:494–548

Lucas R. 1918. Über das Zeitgesetz des kapillaren Aufstiegs von Flüssigkeiten. *Kolloid Zeitschrift* 23:15–22

Ludviksson V, Lightfoot EN. 1971. The dynamics of thin liquid films in the presence of surface-tension gradients. *AIChE J.* 17:1166-73

Makihara M, Sato M, Shimokawa F, Nishida Y. 1999. Micromechanical optical switches based on thermocapillary integrated in waveguide substrate. *J. Lightwave Technol.* 17:14–18

Mann JA, Romero L, Rye RR, Yost FG. 1995. Flow of simple liquids down narrow V grooves. *Phys. Rev. E* 52:3967–72

Maoz R, Sagiv J. 1984. On the formation and

structure of self-assembling monolayers. *J. Colloid Interface Sci.* 100:465–96

Marangoni C. 1871. Ueber die Ausbreitung der Tropfen einer Flüssigkeit auf der Oberfläche einer anderen. *Ann. Phys. Chem.* 143:337–54

Marcelin A. 1925. Les solutions superficielles—Fluides a deux dimensions. *Ann. de Phys.* 4:459–527

Middleman S. 1995. *Modeling Axisymmetric Flows: Dynamics of Films, Jets, and Drops*. San Diego: Academic Press

Moilliet JL, ed. 1963. *Waterproofing and Water-Repellency*. Amsterdam: Elsevier

Möller HG. 1908. Elektrolytische Vorgänge an der Elektrodenoberfläche. Überspannung und Elektrokapillarität. *Z. Phys. Chem.* 65: 226–54

Mori VH, van de Ven TGM, Mason SG. 1982. Resistance to spreading of liquids by sharp edged microsteps. *Coll. Surf.* 4:1–15

Nakata S, Iguchi Y, Ose S, Kuboyama M, Ishii T, Yoshikawa K. 1997. Self-rotation of a camphor scraping on water: new insight into the old problem. *Langmuir* 13:4454–58

Navier CLMH. 1823. Mémoire sur les lois du mouvement des fluids. *Mem. Acad. Roy. Sci. Paris* 6:389–416

Neimark AV, Ruetsch S, Kornev KG, Ravikovitch PI, Poulin P, et al. 2003. Hierarchical pore structure and wetting properties of single-wall carbon nanotube fibers. *Nano Lett.* 3:419–23

Nie XB, Chen SY, E WN, Robbins MO. 2004. A continuum and molecular dynamics hybrid method for micro- and nano-fluid flow. *J. Fluid Mech.* 500:55–64

O'Connell ST, Thompson PA. 1995. Molecular dynamics-continuum hybrid computations: a tool for studying complex fluid flows. *Phys. Rev. E* 52:R5792–95

Ollivier H. 1907. Recherches sur la capillarité. *Ann. Chim. Phys.* 10:229–88

Ottino JM, Wiggins S. 2004. Transport and mixing at the microscale. *Phil. Trans. R. Soc. London A* 362:923–1129

Paalzow A. 1858. Ueber einige Bewegungserscheinungen innerhalb des Schließungsbogens der galvanischen Kette. *Ann. Phys. Chem.* 104:413–21

Pfahler J, Harley J, Bau H, Zemel J. 1990. Liquid transport in micron and submicron channels. *Sens. Actuators* A22:431–34

Pollack MG, Fair RB, Shenderov AD. 2000. Electrowetting-based actuation of liquid droplets for microfluidic applications. *Appl. Phys. Lett.* 77:1725–26

Priezjev NV, Troian SM. 2004. Molecular origin and dynamic behavior of slip in sheared polymer films. *Phys. Rev. Lett.* 92:018302:1–4

Quéré D. 1999. Fluid coating on a fiber. *Annu. Rev. Fluid Mech.* 31:347–84

Quincke G. 1888. Ueber periodische Ausbreitung an Flüssigkeitsoberflächen und dadurch hervorgerufene Bewegungserscheinungen. *Ann. Phys. Chem.* 35:580–642

Raphaël E. 1989. Capillary rise of a wetting fluid in a semi-circular groove. *J. Phys. France* 50:485–91

Lord Rayleigh. 1890. Measurements of the amount of oil necessary in order to check the motions of camphor upon water. *Proc. Roy. Soc. London* 47:364–67

Romero LA, Yost FG. 1996. Flow in an open channel capillary. *J. Fluid Mech.* 322:109–29

Roques-Carmes T, Hayes RA, Feenstra BJ, Schlangen LJM. 2004. Liquid behavior inside a reflective display pixel based on electrowetting. *J. Appl. Phys.* 95:4389–96

Rowlinson JS. 1983. The thermodynamics of a liquid lens. *J. Chem. Soc., Faraday Trans. 2* 79:77–90

Roy RV, Schwartz LW. 1999. On the stability of liquid ridges. *J. Fluid Mech.* 391:293–318

Sammarco TS, Burns MA. 1999. Thermocapillary pumping of discrete drops in microfabricated analysis devices. *AIChE J.* 45:350–66

Schatz MF, Grigoriev RO, Garnier N. 2002. Optical manipulation of microscale fluid flow. *Bull. Am. Phys. Soc.* 47:49 and *Phys. Rev. Lett.* 91:054501-1-4 (2003)

Scriven LE. 1960. Dynamics of a fluid interface-equation of motion for Newtonian surface fluids. *Chem. Eng. Sci.* 12:98–108

Sekimoto K, Oguma R, Kawasaki K. 1987. Morphological stability analysis of partial wetting. *Ann. Phys.* 176:359–92

Shafrin EG, Zisman WA. 1960. Constitutive relations in the wetting of low energy surfaces and the theory of the retraction method of preparing monolayers. *J. Phys. Chem.* 64:519–24

Shibuichi S, Onda T, Satoh N, Tsujii K. 1996. Super water-repellent surfaces resulting from fractal structure. *J. Phys. Chem.* 100:19512–17

Shikhmurzaev YD. 1997. Moving contact lines in liquid/liquid/solid systems. *J. Fluid Mech.* 334:211–49

Shin JY, Abbott NL. 1999. Using light to control dynamic surface tensions of aqueous solutions of water soluble surfactants. *Langmuir* 15:4404–10

Smith MK. 1995. Thermocapillary migration of a two-dimensional liquid droplet on a solid surface. *J. Fluid Mech.* 294:209–30

Smolders CA. 1961. Contact angles—wetting and de-wetting of mercury 3. *Rec. Trav. Chim.* 80:699–720

Spaid MA, Homsy GM. 1996. Stability of Newtonian and viscoelastic dynamic contact lines. *Phys. Fluids* 8:460–78

Stone HA, Stroock AD, Adjari A. 2004. Engineering flows in small devices: microfluidics toward a lab-on-a-chip. *Annu. Rev. Fluid Mech.* 36:381–411

Summ BD, Chadov AV, Raud EA, Goryunov YV. 1980. Laws governing the spreading of liquids over the surface of solids. *Kolloidn. Zh.* 42:1010–14

Thompson PA, Troian SM. 1997. A general boundary condition for liquid flow at solid surfaces. *Nature* 389:360–62

Thorsen T, Maerkl SJ, Quake SR. 2002. Microfluidic large-scale integration. *Science* 298:580–84

Troian SM, Herbolzheimer E, Safran SA, Joanny JF. 1989. Fingering instabilities of driven spreading films. *Europhys. Lett.* 10:25–30

Vallet M, Berge B, Vovelle L. 1996. Electrowetting of water and aqueous solutions on PET insulating films. *Polymer* 37:2465–70

Vallet M, Vallade M, Berge B. 1999. Limiting phenomena for the spreading of water on polymer films by electrowetting. *Eur. Phys. J.* B11:583–91

Volkoviski V. 1935. Sur les tourbillons en festons. *Compt. Rend. Acad. Sci. Paris* 200:1285–87

Washburn EW. 1921. The dynamics of capillary flow. *Phys. Rev.* 17:273–83

Weislogel MM. 1997. Spontaneous capillary flow in partially coated tubes. *AIChE J.* 43:645–54

Weislogel MM, Lichter S. 1998. Capillary flow in an interior corner. *J. Fluid Mech.* 373:349–78

Welters WJJ, Fokkink LGJ. 1998. Fast electrically switchable capillary effects. *Langmuir* 14:1535–38

Xia Y, Yin Y, Lu Y, McLellan J. 2003. Template-assisted self-assembly of spherical colloids into complex and controllable structures. *Adv. Funct. Mater.* 13:907–18

Yarin AL, Liu W, Reneker DH. 2002. Motion of droplets along thin fibers with temperature gradient. *J. Appl. Phys.* 91:4751–60

Annual Review of Fluid Mechanics
Volume 37, 2005

# CONTENTS